Intrinsic Optical and Passive Electrical Properties of Cut Frog Twitch Fibers

MALCOLM IRVING, JAMES MAYLIE, NING LEUNG SIZTO, and W. KNOX CHANDLER

From the Department of Physiology, Yale University School of Medicine, New Haven, Connecticut 06510

ABSTRACT   This article describes a new apparatus for making simultaneous optical measurements on single muscle fibers at three different wavelengths and two planes of linear polarization. There are two modes of operation: mode 1 measures the individual absorbances of light linearly polarized along and perpendicular to the fiber axis, and mode 2 measures retardation (or birefringence) and the average of the two absorbance components. Although some intact frog twitch fibers were studied, most experiments used cut fibers (Hille, B., and D. T. Campbell. 1976. *Journal of General Physiology*. 67:265–293) mounted in a double-Vaseline-gap chamber (Kovacs, L., E. Rios, and M. F. Schneider. 1983. *Journal of Physiology*. 343:161–196). The end-pool segments were usually exposed for 2 min to 0.01% saponin. This procedure, used in subsequent experiments to make the external membranes in the end pools permeable to Ca indicators (Maylie, J., M. Irving, N. L. Sizto, G. Boyarsky, and W. K. Chandler. 1987. *Journal of General Physiology*. 89:145–176; Maylie, J., M. Irving, N. L. Sizto, and W. K. Chandler. 1987. *Journal of General Physiology*. 89:41–143), was routinely employed so that all our cut fiber results would be comparable. A simple method, which does not require microelectrodes, allowed continual estimation of a fiber's membrane (r_m) and internal longitudinal (r_i) resistances as well as the external resistance (r_e) under the Vaseline seals. The values of r_m and r_i obtained from cut fibers with this method agree reasonably well with values obtained from intact fibers using microelectrode techniques. Optical measurements were made on resting and action potential–stimulated fibers. The intrinsic fiber absorbance, defined operationally as $\log_{10}$ of the ratio of incident light to transmitted light intensity, was similar in intact and cut preparations, as were the changes that accompanied stimulation. On the other hand, the resting birefringence and the peak of the active change in cut fibers were, respectively, only 0.8 and 0.7 times the corresponding values in intact fibers. Both the amplitude and the half-width of the active retardation signal increased considerably during the time course of cut fiber experiments; a

Address reprint requests to Dr. W. Knox Chandler, Department of Physiology, 333 Cedar Street, New Haven, CT 06510. Dr. Irving's present address is Department of Biophysics, King's College London, 26-29 Drury Lane, London WC2B 5RL, England. Dr. Sizto's present address is 3154 Waugh Place, Fremont, CA 94536.

twofold increase in 2 h was not unusual. Such changes are probably due to a progressive alteration in the internal state of the cut fibers.

INTRODUCTION

Since the first myoplasmic Ca transient was reported by Jobsis and O'Connor (1966), much effort has been directed toward determining free [Ca] inside muscle cells. Muscle Ca transients may last only 10–20 ms, so that the method of measurement must have good time resolution. Measurements of optical properties of Ca indicators are frequently used for this purpose. These compounds, on complexing Ca, undergo a change, such as in absorbance; in favorable cases, this change can be measured within a fraction of a millisecond. A complete description of the optical signals often requires the use of light of several wavelengths and two planes of linear polarization.

Recent experiments in this laboratory have illustrated this requirement (Baylor et al., 1982a–c; see also Miledi et al., 1982). Isolated twitch fibers were injected with arsenazo III, and changes in absorbance were measured after stimulation. Three different components could be resolved in the optical signals. One component appeared to track myoplasmic Ca; this was best measured using light of wavelength 650–660 nm. A second component was detected when linearly polarized light was used; at certain wavelengths, the change in absorbance for light polarized along the fiber axis was different from that for light polarized perpendicular to this axis. The difference between the two signals, the dichroic signal, was best measured at 570 nm, near the isosbestic wavelength for changes in pH, Mg, or Ca. A third component was intrinsic to the fiber; it was measured at wavelengths where the indicator is transparent (750 nm, for example) and was used to correct signals at other wavelengths to obtain the absorbance changes of the indicator. Thus, in muscle, arsenazo III gives two distinct signals, Ca and dichroic, but the resolution of these signals requires light of at least three different wavelengths (such as 570, 660, and 750 nm) and two planes of linear polarization.

A limitation of the experimental apparatus of Baylor et al. (1982a–c) was that it could measure optical changes at only one wavelength and one plane of linear polarization at a time. Since it would be convenient to make measurements at three wavelengths and two planes of linear polarization simultaneously, we designed and constructed the necessary equipment. With minor modification, this equipment can also simultaneously measure absorbance and retardation (or birefringence); this is useful since, after stimulation, there is a change in fiber retardation, one component of which appears to be related to excitation-contraction coupling (Baylor and Oetliker, 1977a). This article describes the new apparatus and its theory of operation.

The first experiments with this apparatus were carried out on intact fibers injected with arsenazo III. Then Dr. S. M. Baylor told us about recent results which showed that arsenazo III does not track myoplasmic free [Ca] in a simple and rapid fashion. The Ca-related absorbance change consists of at least two components, an early one that tracks free [Ca] rapidly, within 1–2 ms, and a

later one that tracks [Ca] with a delay of ~10 ms (Baylor et al., 1983; Quinta-Ferreira et al., 1984). We therefore decided to try other indicators.

Two of the most promising possibilities, antipyrylazo III and murexide, are difficult to inject into intact fibers. On the other hand, cut fibers (Hille and Campbell, 1976) are easily loaded with antipyrylazo III (Kovacs et al., 1979). They have several other advantages over isolated intact fibers: ease of preparation, high tolerance to repeated depolarization under voltage clamp, and convenient measurement of the extent of binding of indicators to myoplasmic constituents (Maylie et al., 1987b). Consequently, the experimental apparatus used for intact fibers was modified to accommodate cut fibers. This article describes our cut fiber technique, including a simple method for estimating passive electrical properties, which does not require the use of internal micro-electrodes. It also describes some of the intrinsic optical properties of cut fibers and compares them with those of intact fibers.

METHODS

Experimental Chamber

Most experiments used cut muscle fibers (Hille and Campbell, 1976) from cold-adapted *Rana temporaria*. The method of dissection and the experimental chamber were similar to those employed by Kovacs et al. (1983), whose article should be consulted for additional details. A stretched semitendinosus or iliofibularis muscle was exposed to a Ca-free, high-K relaxing solution (Table 1A), which caused a transient contraction followed by relaxation. A 6–12-mm length of a single fiber was then isolated and carefully transferred to a Lucite chamber containing the same relaxing solution. Once in the chamber, the cut fiber segment was attached, either with Vaseline and Scotch tape (Kovacs et al., 1983) or with small Lucite clamps, to mobile pedestals in the two end pools and stretched to a sarcomere spacing of 3.4–4.5 μm. Two Vaseline seals (VS) were then applied to provide electrical isolation between the central pool and the two end pools (Fig. 1). Two Lucite covers, applied to the end pools, provided additional isolation of the solutions.

To introduce Ca indicators into cut fibers from the end-pool solutions, the surface membrane in the end pools was usually made permeable by saponin (Endo and Iino, 1980). The end-pool treatment consisted of a 2-min exposure to relaxing solution containing 0.01% saponin (Sigma Chemical Co., St. Louis, MO), followed by a thorough rinsing with saponin-free relaxing solution. This was then replaced with internal solution (Table 1A). The central-pool solution was changed to either Ringer's or TEA solution (Table 1B). The concentration of saponin and the exposure time were somewhat arbitrary. A 2-min exposure to 0.01% saponin produced fibers that almost always took up the indicator, whereas a 1-min exposure frequently gave fibers that did not. Although Ca indicators were not used in this article, except for the experiment in Fig. 16, the saponin treatment was nonetheless employed, except where indicated, so that these results could be compared with later results obtained from fibers containing an indicator.

In one experiment reported later (Figs. 1 and 6 in Maylie et al., 1987c), notches (N) rather than saponin were used to facilitate indicator entry into the end-pool segments (Fig. 1).

Agar bridges, filled with the appropriate end-pool or central-pool solution, provided electrical connections between each compartment in the chamber and a small side pool filled with 3 M KCl and fitted with an Ag/AgCl pellet. Separate side pools were used to measure voltage and pass current.

TABLE I

Solutions

(A) End-pool solutions

	K-glutamate	PIPES	EGTA	MgSO₄	Glucose	Na₂-ATP	K₂-creatine phosphate
	mM	mM	mM	mM	mM	mM	mM
Relaxing	120	5	0.1	1.0	0	0	0
Internal	75.5	5	0.1	6.8	5	5.5	20

(B) External solutions

	NaCl	TEACl	KCl	RbCl	Na₂HPO₄	NaH₂PO₄	CaCl₂	TTX
	mM	mM	mM	mM	mM	mM	mM	μM
Ringer's	120	0	2.5	0	2.15	0.85	1.8	0
TEA	0	120	0	2.5	2.15	0.85	1.8	1

The pH of the end-pool solution was adjusted to 7.0 by adding KOH. The pH of the external solutions was 7.1. The free Mg concentration in the internal solution was calculated as 1.0 mM.

At the beginning of each experiment, the bridge that normally connects EP_1 to its side pool was temporarily removed, a 3 M KCl agar bridge was placed between the KCl-filled side pools used to measure voltage in the CP and EP_1 compartments, and any residual potential difference was nulled to zero. At the end of the experiment, the measurement was repeated so that electrode drift, usually 0–3 mV, could be assessed.
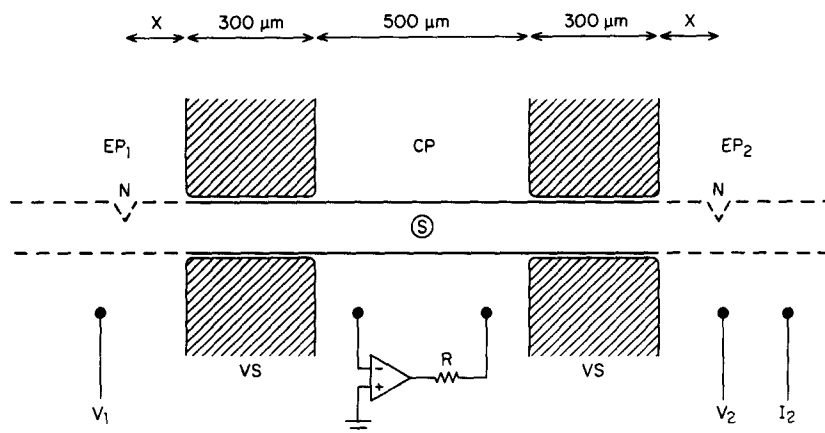

FIGURE 1.   Schematic diagram of the double-gap chamber used for cut muscle fibers. The solution that bathes the fiber is separated into three compartments by two Vaseline seals (VS). EP_1 denotes the left-hand end pool, used for measuring voltage, V_1, and EP_2 denotes the right-hand end pool, used for passing current, I_2, as well as monitoring voltage, V_2. CP denotes the central pool, which was held at earth potential by a high-gain amplifier. The current from the amplifier, which equals I_2, was determined by measuring the voltage across the feedback resistance, R. S denotes the 50-μm spot used for optical recording. The entry of indicator into the fiber in the two end-pool regions was facilitated by either cutting notches (N), usually 100–200 μm (= X) from the Vaseline seals, in the end-pool regions of the fiber, or exposing these regions for 2 min to a solution containing 0.01% saponin (saponin-treated regions are indicated by the dashed lines).

For action potential stimulation, a 0.1–1.0-ms pulse of depolarizing current, I_2, was applied to EP_2 (Fig. 1). This was added to the steady hyperpolarizing current, updated every 5 s by the computer, which was required to maintain V_1, the potential in EP_1, at −90 mV. The amplitude of the action potential was routinely measured using a storage oscilloscope (model 5113, Tektronix, Inc., Beaverton, OR). In some experiments, V_1 was controlled using the voltage-clamp technique. Conventional feedback electronics were employed and the command pulses were rounded by an RC circuit with a 1-ms time constant.

The temperature in the central-pool region was measured with a thermistor (Fenwal Inc., Ashland, MA) positioned near the fiber. A Peltier device (Cambion Div., Midland-Ross Corp., Cambridge, MA), which served as a platform for the chamber, cooled the preparation to 17–19°C.

A few experiments were performed on single intact fibers isolated from the tibialis anterior longus muscle. Silver loops, tied to the tendon ends, were attached to two tungsten hooks mounted on miniature translators. To help reduce movement artifacts, the fiber was stretched to a sarcomere length of 3.7–4.2 μm and lowered onto a 1-mm pedestal. The pedestal, which was in the path of incident light, was cut from a 1.8-mm-thick quartz plate that served as the bottom of the chamber. Two platinum wires, embedded in the quartz plate on either side of the pedestal, were used for action potential stimulation.

Optical Measurements

The optical methods were similar to those used by Baylor et al. (1982a), except that provision was made to measure intensities simultaneously at three different wavelengths and two planes of linear polarization. Fig. 2 shows a diagram of the apparatus, incorporated into a Reichert (Buffalo, NY) research microscope. The shutter (S) and photodiodes (PD) were connected to an 11/23 or 11/73 LSI computer system (Digital Equipment Corp., Marlboro, MA), which controlled the experiment and handled data collection.

Briefly, incident light with a wavelength range of approximately 400–850 nm was focused, using Kohler-type illumination, to a 50-μm spot, 1.5–3.0 W/cm² (measured assuming a photodiode efficiency of 0.45 A/W, EG&G, Electro-Optics Div., Salem, MA), on the fiber. The emerging light was collected and separated into three beams with two beam-splitting cubes (BSC). The three wavelengths for measurement were determined by the three interference filters, λ_1, λ_2, and λ_3; the λ_1 filter could be easily changed during an experiment. Light of each wavelength was split into two beams of orthogonal linear polarization by a polarizing beam-splitting Thompson prism (BST). In most experiments, 10-nm bandpass (i.e., full-width, half-maximum bandpass) filters were used for λ_1 and 30-nm bandpass filters were used for λ_2 and λ_3. Consequently, the λ_2 records, taken with half the transmitted light and a 30-nm bandpass filter, usually contained the least amount of noise, and the λ_1 records, taken with a quarter of the transmitted light and a 10-nm bandpass filter, contained the greatest amount of noise.

Each polarized beam was focused by a lens (L4) onto one of six photodiodes. Each photodiode was connected to an operational amplifier circuit (not shown), which had a feedback resistance of 10 MΩ. Eight electrical signals, from the six photodiodes, from voltage, V_1, and from the voltage across R (which is proportional to I_2, Fig. 1), went to separate instrumentation amplifiers (model 3606AG, Burr-Brown Corp., Tucson, AZ) with a gain of 1–1,024, which could be set by the computer. This stage was usually followed by eight-pole Bessel filters (model ATF76-L8ML, Burr-Brown Corp.) with a cutoff frequency of 0.625, 2.5, or 10 kHz. The eight signals were multiplexed and sampled by a 12-bit A/D converter (model DT2782, Data Translation, Marlboro, MA) working in direct memory access mode. The standard sampling rate was 40 kHz (5 kHz

per channel), although in a few experiments, which will be indicated, 8 or 100 kHz was used. The cutoff frequency of the Bessel filters was usually set to 0.625 kHz.

During an experiment, the shutter was closed, except when measurements of light intensity were being made. At the beginning of a measurement, the voltage from each photodiode amplifier was sampled while the shutter was closed, and then sampled again after the shutter was opened. The difference between the two voltages gave the resting light intensity.

The photodiode circuit was then changed to a sample-and-hold mode of operation in which the resting level of photodiode voltage was subtracted from the ensuing signal and the gain was increased by a factor of 10. In chronological order, baseline data were sampled, the fiber was stimulated electrically, data were collected, and the shutter was closed.

The data were initially processed before being stored. First, since the eight data channels were multiplexed to a single A/D converter, the precise moment of data acquisition differed from one channel to the next by the sample interval. Channels 2–8 were synchronized to channel 1 by linear interpolation. Second, each trace was compressed by a factor of 2 by keeping every other point calculated as an average (1:2:1) of the original
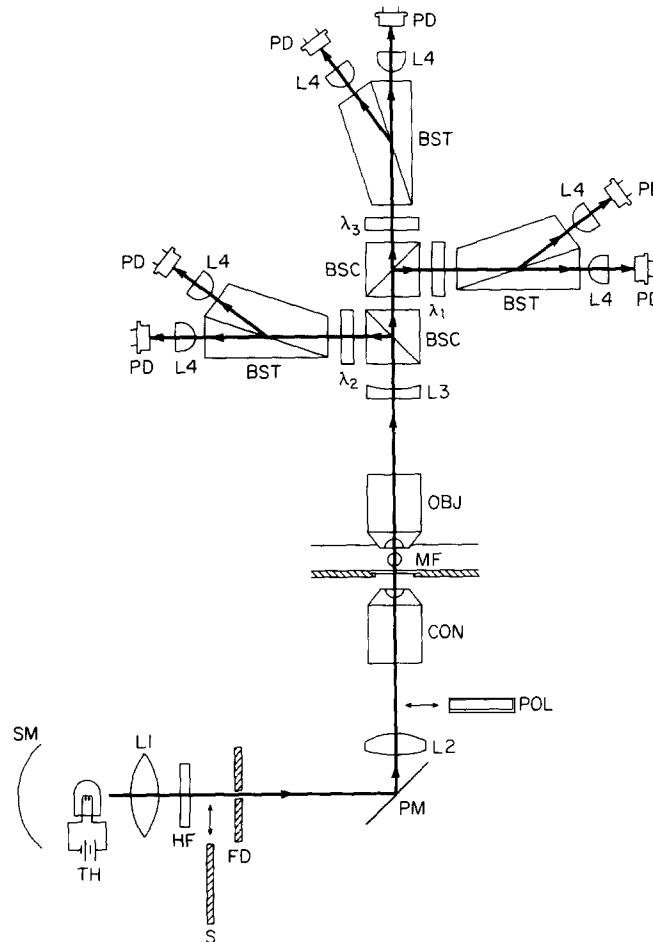
(previous:present:next) points. Third, during the final time course of a signal, when changes are slow, only every fifth point of the 1:2:1 trace was kept. This point was obtained by quadratically smoothing the original 1:2:1 point and the three points on either side of it (Hamming, 1977, p. 34). All traces in this and the three articles that follow (Maylie et al., 1987*a–c*) represent single sweeps; signal averaging was not used.

The apparatus described in Fig. 2 was used in two different configurations, as diagrammed in Fig. 3. Mode 1 was used to measure the absorbance of light linearly polarized both along and perpendicular to the fiber axis. Mode 2 was used to measure optical retardation as well as average absorbance, i.e., the absorbance that would be measured with unpolarized light. Mode 2 therefore gives less complete information about absorbance than mode 1 and was used only when measurements of optical retardation were required. These two modes of operation are described below.

Mode 1. In mode 1 (Fig. 3), unpolarized incident light was focused on a muscle fiber (MF) lying in the plane of the paper (strictly speaking, a small linear polarization preference was present owing to the shape of the lamp filament). At each wavelength, the transmitted light was split by the beam-splitting Thompson prism into components polarized linearly along the fiber axis (0° light) and perpendicular to the fiber axis (90° light).

Since measurements of the absorbance of Ca indicators were planned, light intensities were routinely expressed in terms of absorbance, A, according to the usual formula:

$$A_\theta = \log_{10}[I_\theta(i)/I_\theta(t)]. \tag{1}$$

FIGURE 2. (*opposite*) Schematic diagram of the optical apparatus used to measure simultaneously the intensity of transmitted light at three different wavelengths and two planes of linear polarization. SM, spherical mirror. TH, 100-W tungsten-halogen lamp powered by a stabilized power supply (model ATE 15-15M, Kepco, Inc., Flushing, NY). L1, collecting lens (Schoeffel Instrument Co.). HF, heat filter (Schott Glass Technologies, Inc., Duryea, PA) or cold window (Omega Optical, Inc., Brattleboro, VT) plus, sometimes, a cut-on filter (Schott Glass Technologies). S, shutter for limiting exposure of the preparation to light. FD, field diaphragm for providing a spot of illumination on the preparation. PM, plane mirror. L2, tube lens (300-mm spherical achromatic doublet, Melles Griot, Irvine, CA) for producing a parallel beam. POL, plastic polarizer (Polaroid Corp., Cambridge, MA) for producing linearly polarized light in mode 2 operation (Fig. 3). CON, condenser objective (H20 infinity-corrected objective, magnification 20×, NA 0.4, E. Leitz, Inc., Rockleigh, NJ) for focusing light onto the fiber. MF, muscle fiber placed in experimental chamber with a 170–180-μm glass coverslip at the bottom (although the lens condenser objective is designed for use with a 1.8-mm quartz coverslip, it was verified both theoretically and experimentally that extremely good optical resolution can be obtained with the thin glass coverslip and a 1.9-mm path of aqueous solution between the coverslip and the muscle fiber). OBJ, water immersion objective (25×, NA 0.6, E. Leitz, Inc.) for collecting transmitted light. L3, tube lens (50-mm plano-concave lens, Melles Griot) for producing a parallel beam. BSC, beam-splitting cube (Karl Lambrecht Corp., Chicago, IL) for separating light into two beams. λ_1, λ_2, and λ_3, three-cavity interference filters with 10- or 30-nm bandpass (Ditric Optics, Inc., Hudson, MA). BST, beam-splitting Thompson prism (Karl Lambrecht Corp.) for splitting the incoming light into two beams, one linearly polarized in the plane of the diagram (deviated beam) and one linearly polarized perpendicular to the diagram (undeviated beam). L4, lens (18-mm plano-convex lens, Melles Griot) to focus light onto PD, a photodiode (UV-100B, EG&G).

The intensities of incident and transmitted light are denoted by $I(i)$ and $I(t)$, respectively; θ (= 0 or 90) refers to 0° or 90° light. Absorbance defined in this manner includes contributions from light scattering (including reflection, refraction, and diffraction) as well as true absorbance. The incident light intensity was very stable; in 50 experiments, it decreased, on average, to 0.9946 of its initial value in 154 min, with a standard deviation of 0.0057.
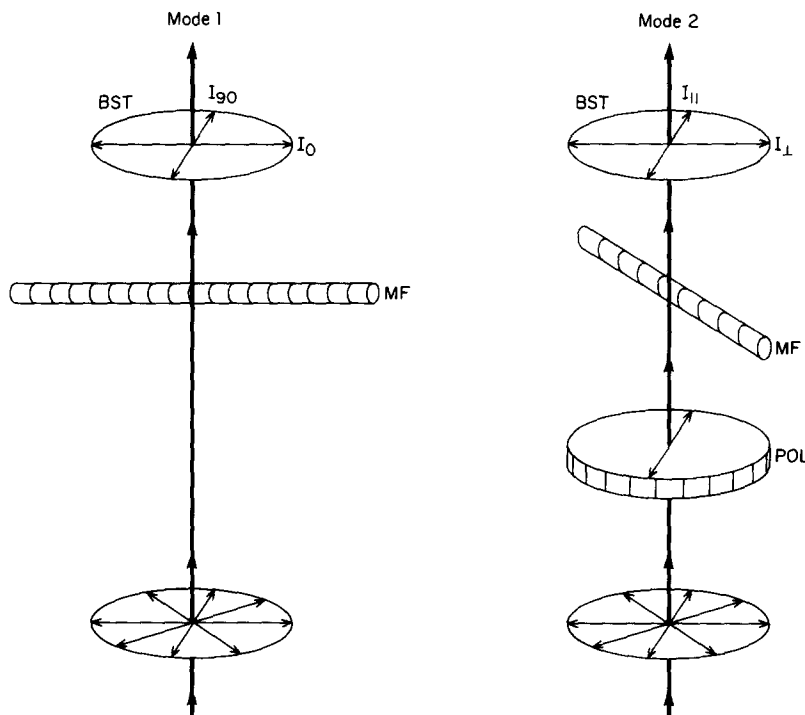

FIGURE 3.   Schematic illustrations of the two modes of operation of the apparatus in Fig. 2. Measurements in mode 1 give the absorbance of light linearly polarized at 0° and 90° with respect to the fiber axis. Measurements in mode 2 give the average absorbance (i.e., the average of values for 0° and 90° polarized light) and optical retardation. See text for additional details.

Changes in absorbance, ΔA, are given by the differential form of Eq. 1:

$$\Delta A_\theta = -\frac{1}{\ln(10)} \cdot \Delta I_\theta(t)/I_\theta(t). \qquad (2)$$

Experimental results are frequently expressed as a linear combination of A_0 and A_{90} (or, correspondingly, ΔA_0 and ΔA_{90}):

(i) $A(1:1) = [A_0 + A_{90}]/2$. This is the average absorbance that would be measured with unpolarized light.

(ii) $A(\delta) = A_0 - A_{90}$. This difference is the linear dichroism. A nonzero value implies that some of the absorbing structures or molecules are not randomly oriented.

(iii) $A(1:2) = [A_0 + 2A_{90}]/3$. If the absorbing structures or molecules are all randomly oriented, A_0 is equal to A_{90}. In the presence of dichroism, however, A_{90} is different from A_0. For a cell such as muscle, with radial symmetry, it can be shown that $A(1:2)$ gives the

absorbance that would be measured if the absorbing structures were randomly oriented (Baylor et al., 1982c); i.e., $A(1:2)$ is not influenced by orientation or changes in orientation.

Mode 2. For mode 2 operation, a linear polarizer (POL in Fig. 2) was placed in the light path to polarize the incident light in the direction perpendicular to the plane of the paper (Fig. 3). The muscle fiber was oriented at 45° with respect to this plane. The beam-splitting Thompson prism separated the transmitted light into components polarized parallel (‖ light) and perpendicular (⊥ light) to the incident beam. This arrangement of polarization elements is similar to that employed by Eberstein and Rosenfalck (1963), except that they measured the intensity of ‖ and ⊥ light in separate runs, after rotating an analyzer 90°.

In mode 2, the relationship between the intensities of incident and transmitted light depends on the amount of optical retardation, R, introduced by the fiber as well as on the absorbances A_0 and A_{90}. Values of R and $A(1:1)$ can be determined from these intensities using the theory given in the Appendix of Baylor et al. (1984). According to their Eqs. A20 and A16, $I_\parallel(t)$ and $I_\perp(t)$ are given by the relationships

$$I_\parallel(t)/I_\parallel(i) = \frac{10^{-A(1:1)}}{2} \cdot [\cosh(\xi) + \cos(\phi)], \tag{3}$$

$$I_\perp(t)/I_\parallel(i) = \frac{10^{-A(1:1)}}{2} \cdot [\cosh(\xi) - \cos(\phi)], \tag{4}$$

with

$$\xi = \frac{\ln(10)}{2} \cdot A(\delta). \tag{5}$$

ϕ represents the phase shift between transmitted light polarized along and perpendicular to the fiber axis and is related to optical retardation, R, by the formula

$$\phi = 2\pi R/\lambda, \tag{6}$$

in which λ denotes wavelength.

$A(1:1)$ and R can be estimated from $I_\parallel$ and $I_\perp$ by combining Eqs. 3 and 4. For $A(1:1)$, the equations are simply added to give

$$A(1:1) = \log_{10}[\cosh(\xi)] + \log_{10}\left[\frac{I_\parallel(i)}{I_\parallel(t) + I_\perp(t)}\right]. \tag{7}$$

Changes in $A(1:1)$ are given by the differential form of Eq. 7:

$$\Delta A(1:1) = \frac{1}{\ln(10)} \cdot \left[\tanh(\xi)\Delta\xi - \frac{\Delta I_\parallel(t) + \Delta I_\perp(t)}{I_\parallel(t) + I_\perp(t)}\right]. \tag{8}$$

In all previous reports of the use of Ca indicators in muscle and in our own experiments (Maylie et al., 1987a-c), the measured values of $A(\delta)$ and $\Delta A(\delta)$ have been sufficiently small that the $\cosh(\xi)$ term can be taken as 1 and the $\tanh(\xi)\Delta\xi$ term can be ignored; for example, in the experiments described in Baylor et al. (1982a, c), $|A(\delta)| < 0.03$ and $|\Delta A(\delta)| < 0.002$. Thus,

$$A(1:1) \approx \log_{10}\left[\frac{I_\parallel(i)}{I_\parallel(t) + I_\perp(t)}\right] \tag{9}$$

and

$$\Delta A(1:1) \approx -\frac{1}{\ln(10)} \cdot \frac{\Delta I_\parallel(t) + \Delta I_\perp(t)}{I_\parallel(t) + I_\perp(t)}. \tag{10}$$

The phase shift ϕ can be obtained by taking the difference between Eqs. 3 and 4, and then dividing by the sum:

$$\cos(\phi) = \cosh(\xi) \cdot \frac{I_\parallel(t) - I_\perp(t)}{I_\parallel(t) + I_\perp(t)}. \tag{11}$$

For $|A(\delta)| < 0.03$, the $\cosh(\xi)$ term is sufficiently close to unity that Eq. 11 can be replaced with

$$\cos(\phi) \approx \frac{I_\parallel(t) - I_\perp(t)}{I_\parallel(t) + I_\perp(t)}. \tag{12}$$

Changes in phase shift are given by rearranging the differential form of Eq. 11, and then making the approximations $\cosh(\xi) \approx 1$ and $\tanh(\xi) \approx \xi$:

$$\Delta\phi \approx \frac{\sin(\phi)}{2} \cdot \left[\frac{\Delta I_\perp(t)}{I_\perp(t)} - \frac{\Delta I_\parallel(t)}{I_\parallel(t)} \right] - \frac{\xi\Delta\xi}{\tan(\phi)}. \tag{13}$$

Measurements of $|\Delta R|$ that accompany action potential stimulation have peak values of 0.1–0.6 nm (Baylor and Oetliker, 1977b; Table IV of this article), which, for $500 < \lambda < 800$ nm, give a range of 0.0008–0.008 for $\Delta\phi$. The upper limits given above for $|A(\delta)|$ and $|\Delta A(\delta)|$ correspond to $|\xi\Delta\xi| < 0.00008$. In most experiments, $\tan(\phi)$, for the wavelengths employed, was greater than or approximately equal to 1, so that the second term on the right-hand side of Eq. 13 was much smaller in magnitude than the first term. In this case, the following approximation can be used:

$$\Delta\phi \approx \frac{\sin(\phi)}{2} \cdot \left[\frac{\Delta I_\perp(t)}{I_\perp(t)} - \frac{\Delta I_\parallel(t)}{I_\parallel(t)} \right]. \tag{14}$$

The three beam-splitting cubes (Fig. 2) transmit (and reflect) different fractions of $\parallel$ and $\perp$ light. These fractions were determined experimentally for each light path, and correction factors were introduced in applying Eqs. 7–12 to mode 2 records. These factors are not required in the analysis of mode 1 measurements (Eqs. 1 and 2) or in determining $\Delta\phi$ with Eq. 14, apart from the use of $\sin(\phi)$ as a scaling factor.

RESULTS

Electrical Measurements

Passive electrical properties of cut fibers. In the following analysis, V_1 denotes voltage in the voltage-measuring end pool, EP_1, and V_2 and I_2 denote voltage and current in the current-passing end pool, EP_2 (Fig. 1).

After a fiber was mounted in the double-Vaseline-gap chamber and the end-pool regions were treated with 0.01% saponin for 2 min to make them permeable, the bathing solutions were replaced by internal solution in the end pools and by Ringer's or TEA solution in the central pool (Table I). 3–13 min later, electrical recording was begun. Fig. 4A shows the first measurements of V_1 recorded in the absence of current I_2 [called $V_1(I_2 = 0)$] plotted against fiber diameter. Data are shown from 55 fibers in Ringer's solution on which a complete steady state cable analysis was done. The value of $V_1(I_2 = 0)$ varied from -22 to -53 mV, with an average value of -36.5 mV, and showed little correlation with fiber diameter. These values are substantially less negative than the normal resting potential, approximately -90 mV. This depolarization occurs because the finite

external resistance under the two Vaseline seals (VS in Fig. 1) allows the depolarized end-pool segments of a fiber to electrically shunt the membrane in the central pool.

1–2 min after the measurements in Fig. 4A were made, V_1 was set to -90 mV by injecting the necessary current, I_2, into the current-passing end pool. Experi-
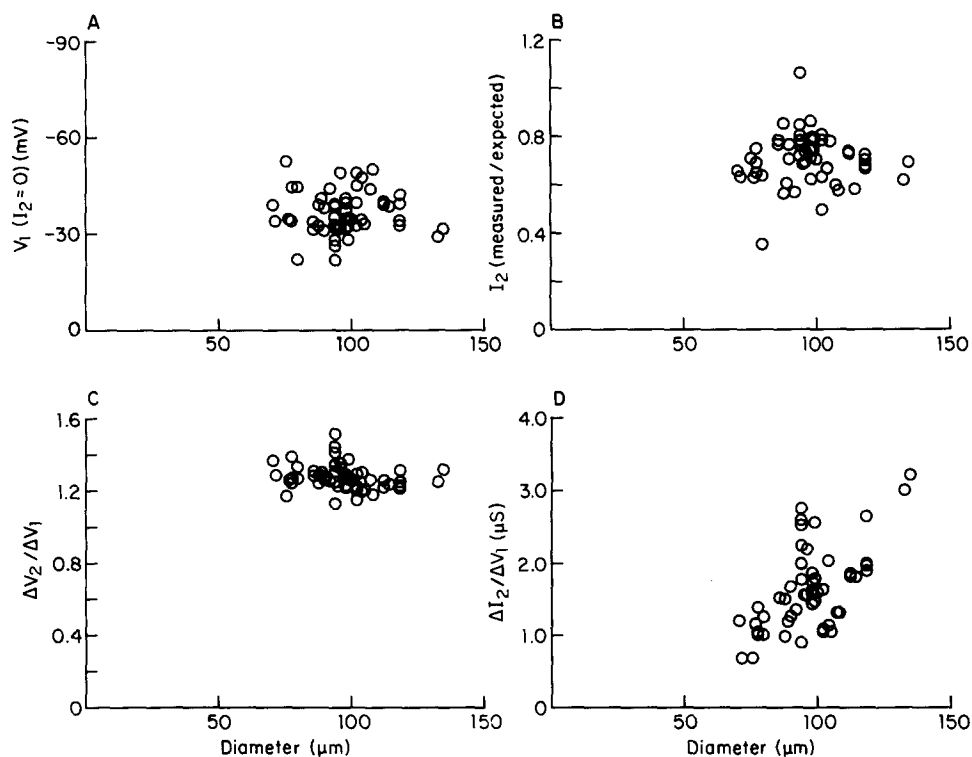

FIGURE 4. Electrical parameters, measured in the double-Vaseline-gap chamber, plotted against fiber diameter, Ringer's solution. (A) End-pool potential, V_1, measured in the absence of applied current (i.e., $I_2 = 0$). The measurements were made, on average, 8 min after the fiber was mounted and the end-pool regions were treated with saponin. (B) Ratio of the actual holding current at $V_1 = -90$ mV to that predicted from Eq. 18, using the results in A, C, and D. (C and D) Measurements of $\Delta V_2/\Delta V_1$ ($= a_1$) and $\Delta I_2/\Delta V_1$ ($= a_2$) associated with a 200–400-ms pulse of amplitude approximately -20 mV in V_2. These measurements, as well as those of holding current used in B, were made, on average, 12 min after those in A. The central pool contained Ringer's solution and the end pools contained internal solution. Sarcomere spacing, 3.5–4.2 μm; average temperature, 18.3°C. See text for additional details.

ments were terminated, and were not included in Fig. 4A, if the magnitude of I_2 either exceeded 0.2 μA or was not stable but progressively increased with time. Otherwise, after about 5–15 min, the exact values of V_2 and I_2 were recorded. If the steady state passive electrical behavior of the system is linear, V_2 and I_2 are related to V_1 in the following way:

$$V_2 = a_1 V_1 + b_1, \tag{15}$$

$$I_2 = a_2 V_1 + b_2, \tag{16}$$

where a_1, a_2, b_1, and b_2 are constants that do not depend on voltage or current.

The following argument shows that these four constants are not independent. Without external current, $I_2 = 0$ and consequently Eq. 16 becomes $a_2 V_1 = -b_2$. Symmetry requires that V_1 and V_2 be equal, so that Eq. 15 becomes $(1 - a_1)V_1 = b_1$. Combining these two expressions gives

$$b_1 = (a_1 - 1)b_2/a_2. \tag{17}$$

Consequently, measurements of three independent quantities are sufficient to describe the system.

From a holding potential $V_1 = -90$ mV, the two constants a_1 and a_2 were routinely determined by imposing a 200–400-ms pulse of amplitude approximately -20 mV in V_2 and measuring ΔV_2, ΔI_2, and ΔV_1. The ratio $\Delta V_2/\Delta V_1$ gives a_1 (Fig. 4C) and $\Delta I_2/\Delta V_1$ gives a_2 (Fig. 4D). The ratio $\Delta V_2/\Delta V_1$ changed little with fiber diameter, whereas the apparent input conductance, $\Delta I_2/\Delta V_1$, increased.

The third independent constant, b_1 or b_2, can be determined either from $V_1(I_2 = 0)$ or from the later measurement of holding current made when a_1 and a_2 were determined [called $I_2(V_1 = -90$ mV)]. For a linear system, Eq. 16 requires that

$$I_2(V_1 = -90 \text{ mV}) = a_2[-90 \text{ mV} - V_1(I_2 = 0)]. \tag{18}$$

Fig. 4B shows a plot of the ratio of the measured holding current, $I_2(V_1 = -90$ mV), to the predicted holding current (the right-hand side of Eq. 18). On average, the measured value was 0.705 times that predicted.

Some of this discrepancy may be due to the 3–13-min depolarization in Ringer's solution that preceded the measurement of $V_1(I_2 = 0)$. During this time, the ionic composition of the myoplasm may have become different from that in an intact fiber at -90 mV; for example, the fiber may have gained Cl. Any such changes should have been reversed later when V_1 was set to -90 mV and $I_2(V_1 = -90$ mV), a_1, and a_2 were measured.

Another possible reason for the discrepancy in Fig. 4B is electrical nonlinearity of the membrane. Any such nonlinearity owing to K channels should be much reduced in TEA solution (Stanfield, 1970; Table 1B). Fig. 5 shows measurements, similar to those in Fig. 4, made on 13 fibers with TEA solution in the central pool. The ratio of measured to predicted holding current in this solution (Fig. 5B) had an average value of 0.94 compared with 0.705 in Ringer's solution.

Eq. 18, then, gives a more accurate prediction of holding current in TEA solution than in Ringer's. Since this difference may be caused by a voltage-sensitive K conductance that is blocked by TEA, we decided to determine b_1 and b_2, in both Ringer's and TEA solution, from the holding current $I_2(V_1 = -90$ mV) rather than $V_1(I_2 = 0)$. Consequently, the three independent parameters a_1, a_2, and b_2 (calculated from the holding current using Eq. 16) were determined from measurements made close to -90 mV; b_1 was calculated from Eq. 17.

The Appendix shows how, using simple assumptions, the constants a_1, a_2, and b_2 can be calculated from three cable parameters: r_m, the fiber membrane

resistance for unit length; r_i, the internal resistance per unit length; and r_e, the external resistance under the Vaseline seals per unit length. Conversely, r_m, r_i, and r_e can be calculated, using an iterative computer program, from a_1, a_2, and b_2. Fig. 6 shows the values of cable parameters in Ringer's solution determined from the constants in Fig. 4.

Fig. 6A shows r_m plotted against the reciprocal of fiber diameter, d. Although the data show scatter, the smaller fibers appear to have a larger membrane resistance for unit length. If ionic conductance were confined to the surface
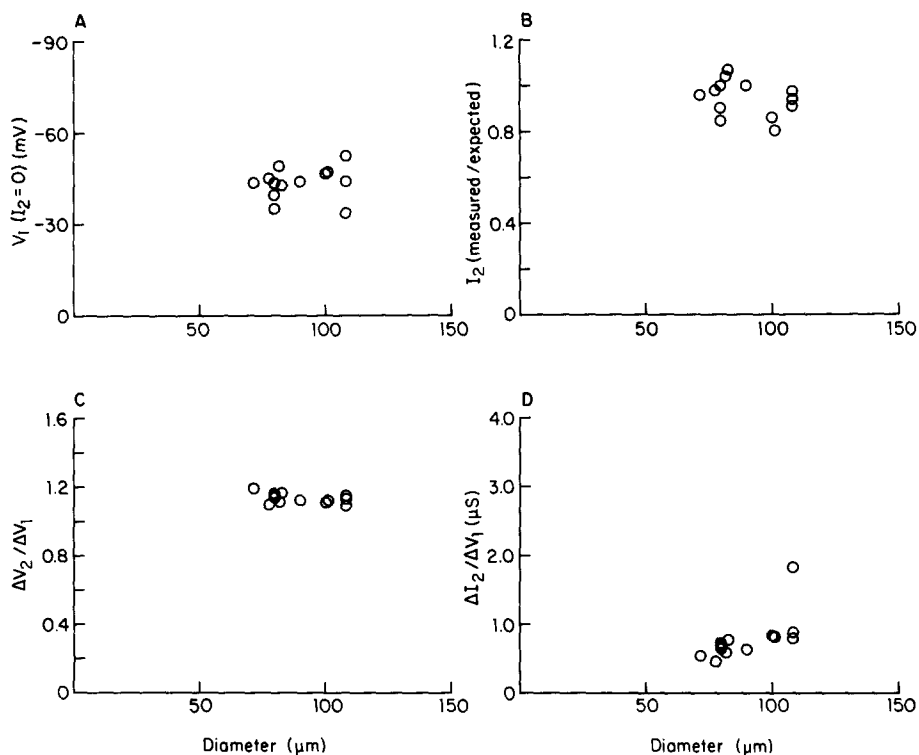

FIGURE 5. Electrical parameters, measured in the double-Vaseline-gap chamber, plotted against fiber diameter, TEA solution. The experimental design was similar to that in Fig. 4 except that the central pool contained TEA solution. The measurements in A were made, on average, 11 min after saponin treatment; the other measurements were made 10 min later. Sarcomere spacing, 3.4–4.1 μm; average temperature, 18.5°C.

membrane, and if fibers of different diameter had the same value of specific membrane resistance, R_m, then r_m would depend linearly on $1/d$. The straight line in Fig. 6A represents a least-squares fit with $R_m = 2,660$ $\Omega \cdot cm^2$. A similar analysis of the TEA results (Fig. 7A) gives $R_m = 5,581$ $\Omega \cdot cm^2$. If, on the other hand, a substantial part of the ionic conductance were located in the membranes of the transverse tubules, the relationship between r_m and $1/d$ would be curvilinear, with a slope that progressively increases as $1/d$ increases. The data in Figs. 6A and 7A seem consistent with this possibility.

Experimental work on intact fibers, reviewed by Adrian (1983), gives a value of ~4,000 $\Omega \cdot cm^2$ for R_m in Ringer's solution. This net resistance is determined by the resistances to K ions, ~12,000 $\Omega \cdot cm^2$, and Cl ions, ~6,000 $\Omega \cdot cm^2$, acting in parallel. The value of 2,660 $\Omega \cdot cm^2$ for R_m in cut fibers in Ringer's solution is
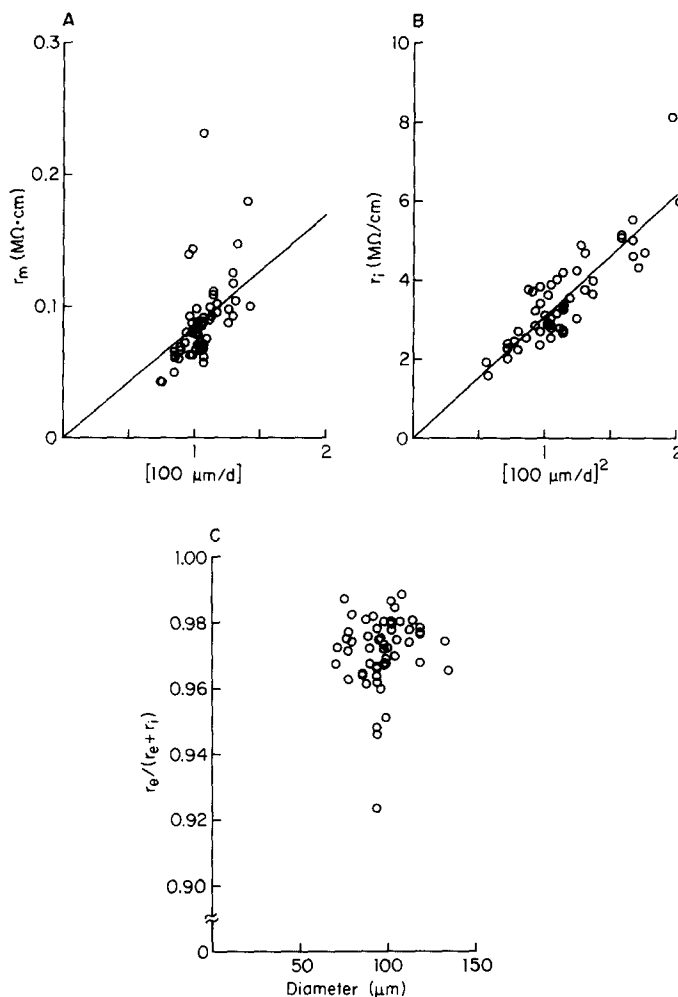

FIGURE 6. Estimates of passive electrical properties of muscle fibers in Ringer's solution. The measurements in Fig. 4 were analyzed using the theory in the Appendix (Eq. A30) in which the reversal potential, V_r, varies linearly with distance under the Vaseline seals. (A) r_m is plotted against (100 μm)/d, where d, fiber diameter, is given in microns. The straight line represents a least-squares fit with the specific resistance of the membrane $R_m = 2,660$ $\Omega \cdot cm^2$. (B) r_i is plotted against $[(100 \ \mu m)/d]^2$. The straight line represents a least-squares fit with the internal specific resistance $R_i = 242$ $\Omega \cdot cm$. (C) The ratio $r_e/(r_e + r_i)$ is plotted against d. The average value is 0.971.

somewhat smaller than the value for intact fibers, ~4,000 $\Omega \cdot cm^2$. In TEA solution, in which the K conductance is nearly abolished, the value of 5,581 $\Omega \cdot cm^2$ for R_m in cut fibers is similar to that expected in intact fibers for the resistance to Cl ions alone, ~6,000 $\Omega \cdot cm^2$. The better agreement in TEA solution
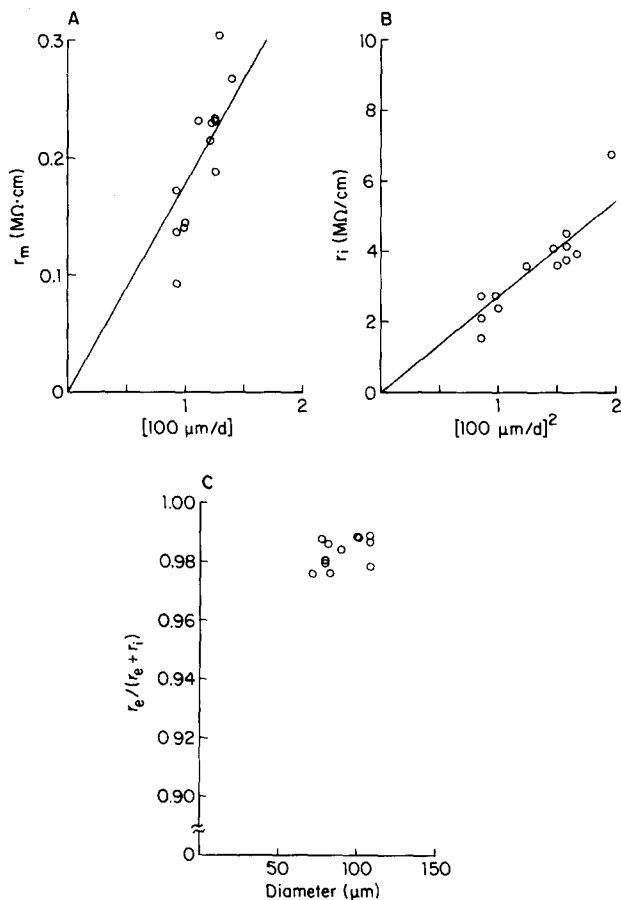

FIGURE 7. Estimates of passive electrical properties of muscle fibers in TEA solution. Similar to Fig. 6. The straight lines in A and B are least-squares fits with R_m = 5,581 $\Omega \cdot cm^2$ and R_i = 214 $\Omega \cdot cm$, respectively. The average value in C is 0.983.

(also compare Figs. 5B and 4B) may be partly due to removal of nonlinear K currents, both in the central region and under the Vaseline seals.

Fig. 6B shows r_i plotted against $1/d^2$ for fibers in Ringer's solution. The straight line is a least-squares fit corresponding to a value of 242 $\Omega \cdot cm$ for R_i, the internal specific resistance. The value for fibers in TEA solution was 214 $\Omega \cdot cm$ (Fig. 7B). These values are slightly greater than that estimated for intact fibers at 18°C, 180 $\Omega \cdot cm$, using R_i = 169 $\Omega \cdot cm$ at 20°C and Q_{10} = 0.73 (Hodgkin

and Nakajima, 1972). They are also slightly greater than the average value, 204 $\Omega \cdot cm$, reported by Hille and Campbell (1976) for cut fibers studied at 5°C.

Figs. 6C and 7C show $r_e/(r_e + r_i)$ plotted against d. This ratio is a measure of the quality of the Vaseline seals; it is equal to the measured voltage in the end pool, V_1, divided by the true membrane potential in the central pool next to the Vaseline seal that adjoins EP_1 (Appendix Eq. A4 with $I_1 = 0$). The average value was 0.971 in Ringer's solution (Fig. 6C) and 0.983 in TEA solution (Fig. 7C). The range of values, 0.92–0.99, lies within the range estimated by Kovacs et al. (1983), 0.8–1.0.

The general conclusions from these results are that the method for estimating linear cable properties works reasonably well, especially for fibers in TEA solution, and that the passive electrical properties of cut fibers, for the most part, are similar to those previously reported for intact fibers.

TABLE II
Cable Parameters in Cut Muscle Fibers

(1) Solution used	(2) Assumed V_r	(3) R_m	(4) R_i	(5) $r_e/(r_e + r_i)$
		$\Omega \cdot cm^2$	$\Omega \cdot cm$	
Ringer's	V_{RP}	3,040	244	0.967
Ringer's	$(x/L_1) \cdot V_{RP}$	2,660	242	0.971
Ringer's	0	1,912	237	0.984
TEA	V_{RP}	6,363	214	0.981
TEA	$(x/L_1) \cdot V_{RP}$	5,581	214	0.983
TEA	0	4,019	211	0.989

Column 1 gives the external solution in the central region and column 2 gives the assumption made about V_r and its dependence on position under the Vaseline seal. The values in columns 3–5 were obtained from least-squares fits of r_m vs. $1/d$ and r_i vs. $1/d^2$ and from the average value of $r_e/(r_e + r_i)$ (Figs. 6 and 7); r_m, r_i, and r_e were calculated from the data in Figs. 4 and 5 using the theory given in the Appendix. Eq. A30 was used for $V_r = (x/L_1) \cdot V_{RP}$ and Eq. A31 was used for constant V_r. V_{RP} was taken to be −90 mV. On average, the measurements in Ringer's solution were made at 18.3°C, 20 min after saponin treatment; those in TEA solution were made at 18.5°C, 22 min after saponin treatment.

Effect of different assumptions concerning the reversal potential under the Vaseline seals. The estimates of cable parameters shown in Figs. 6 and 7 were obtained on the assumption that V_r, the reversal potential for membrane under the Vaseline seals (VS in Fig. 1), varied from zero next to the end pools, which contained high-K internal solution, to −90 mV next to the central pool, which contained low-K Ringer's or TEA solution. For mathematical convenience, a linear spatial variation across the seals was assumed. Calculations were also made with constant V_r; this was set to either 0 or −90 mV, values that should bracket the actual V_r. The results are given in Table II. The estimates of R_m (or r_m) changed appreciably with different assumptions about V_r, whereas those of R_i (or r_i) and $r_e/(r_e + r_i)$ did not.

Electrical measurements: action potential. The traces labeled a in Fig. 8, A and B, show the same voltage record, plotted on different time bases, obtained

from a conventional KCl-filled microelectrode inserted into a fiber in the central region near the EP_1 Vaseline seal. The traces labeled *b* show the same record superimposed on a voltage record, V_1, taken from EP_1. The microelectrode signal was scaled by a factor of 0.977 so that its peak amplitude would match
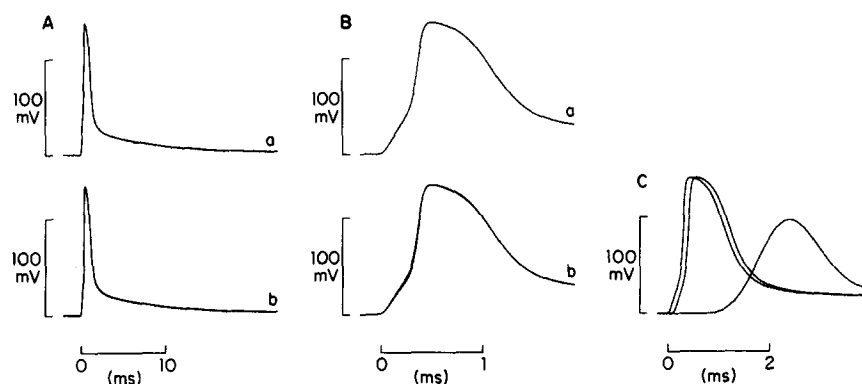

FIGURE 8. Action potential measurements using the double-Vaseline-gap chamber. Trace *a* in panel *A* shows the voltage recorded from a microelectrode inserted into the fiber in the central-pool region ~50 μm from the edge of the Vaseline seal next to EP_1. The electrode, filled with 3 M KCl, had a resistance of 4 MΩ in Ringer's solution at room temperature. The microelectrode made a 20° angle with the horizontal so that it would fit under the water immersion objective. Because of this shallow incline, the distal 1 cm or so of the microelectrode was covered by the central-pool solution, held at earth potential. To avoid the slowing of response that the capacitance across the microelectrode wall would normally produce, the microelectrode was shielded by a coating of Ag paint driven with the unity gain output from the microelectrode amplifier; the Ag paint was insulated by M-coat D (Micro-measurements, Romulus, MI) and fingernail polish. The peak amplitude of the action potential was 137.2 mV. The traces labeled *b* in panel *A* show two superimposed action potentials, one with a peak amplitude of 134.0 mV recorded from end pool EP_1 and the other from the microelectrode, trace *a*, scaled by 0.977. The traces in *B* are similar to those in *A* except for the difference in time base. All records in *A* and *B* were taken with a 10-kHz eight-pole Bessel filter. Fiber diameter, 88 μm; sarcomere spacing, 3.7 μm; Ringer's solution; temperature, 19.4°C; holding potential, −90 mV; time after saponin treatment, 30 min; fiber 101084.2. The action potential traces in *C* were recorded from end pool EP_1 in a different fiber. The first record was taken without a Bessel filter, the middle record with a 10-kHz eight-pole Bessel filter, and the last record with a 0.625-kHz eight-pole Bessel filter. Fiber diameter, 73 μm; sarcomere spacing, not recorded; Ringer's solution; temperature, 17.9°C; holding potential, −90 mV; time after saponin treatment, 25 min; fiber 100584.2. In the experiments in Figs. 8 and 9, only one channel of data was sampled at a time, at a sampling rate of 100 kHz.

that of the end-pool signal. According to linear cable theory (Eq. A4 with $I_1 = 0$), this factor should equal $r_e/(r_e + r_i)$, which is estimated to be 0.965 using the procedure described above. These two values are in good agreement.

In most experiments, voltage and optical signals were filtered before being sampled by the A/D converter (see p. 5 for more details). Fig. 8C shows the

effect of different filters on the action potential. End-pool (EP₁) signals were sampled using no filter (first trace), a 10-kHz, eight-pole Bessel filter (second trace), and a 0.625-kHz, eight-pole Bessel filter (third trace). A Bessel filter introduces a constant time delay for low-frequency components of a signal; high-frequency components are also delayed, but to a lesser degree, and are attenuated. With an eight-pole filter, the constant low-frequency delay is equal to the reciprocal of the cutoff frequency. The middle trace in C shows an accurate temporal waveform of the action potential, but delayed by 0.1 ms as expected for the 10-kHz filter. The last trace shows marked attenuation and is included in the comparison because the 0.625-kHz filter was used routinely in runs involving optical measurements; this filter produced no noticeable attenuation of the optical records (see Fig. 16).

In all figures, the origin of the time base corresponds to the initiation of electrical stimulation, whether by an action potential shock or by a voltage-clamp step, shifted by the low-frequency time delay expected for the Bessel filter. Thus, the $t = 0$ marker in Fig. 8, A and B (10-kHz filter), was placed 0.1 ms after the current pulse was started. No delay was used in C.

End-pool (EP₁) action potentials were measured in a total of 51 fibers held at −90 mV. The average amplitude 10–42 min (average value, 21 min) after saponin treatment was 133.8 mV (range, 127–144 mV; average temperature, 18.3°C), which corresponds to an average overshoot of +43.8 mV. These EP₁ values should be divided by $r_e/(r_e + r_i)$ to give true values of membrane potential. The average ratio in Ringer's solution, 0.971, gives −92.7 mV for the resting potential, 137.8 mV for the amplitude of the action potential, and +45.1 mV for the overshoot. These numbers are similar to those obtained with microelectrodes in intact sartorius fibers at 20°C, where, on average, the resting potential is −88 mV, the action potential amplitude is 129 mV, and the overshoot is +41 mV (Persson, 1963).

Electrical measurements: voltage clamp. Fig. 9 shows voltage records associated with a 20-ms hyperpolarization from a holding potential of −90 mV in Ringer's solution. In A, the trace of larger final amplitude (−51.6 mV) was recorded with a microelectrode, just after insertion into the central region of the fiber near the EP₁ Vaseline seal. The smaller-amplitude trace (−50.3 mV) was measured 28 s later in EP₁ (Fig. 1). As mentioned in the preceding section, the ratio 50.3/51.6 = 0.975 should correspond to $r_e/(r_e + r_i)$, which is equal to 0.977 according to the linear cable analysis. These two values are in good agreement.

After the records in Fig. 9A were obtained, the microelectrode was withdrawn and inserted near the EP₂ Vaseline seal. Then, 5 min after the measurements in Fig. 9A, the voltages were measured again (Fig. 9B). The final amplitude measured with the microelectrode was larger than before, although the EP₁ potential was unchanged. Finally, the microelectrode was withdrawn and reinserted near the EP₁ Vaseline seal to make a bracketing measurement (not shown). During the course of the experiment, the change in potential measured with the microelectrode slowly declined. The first measurements, near EP₁, gave −51.6 mV just after insertion of the microelectrode and −51.4 mV just before with-

drawal. The second set of measurements, near EP_2, gave -53.6 mV just after insertion and -53.0 mV just before withdrawal. The third set of measurements, near EP_1, gave -50.7 mV just after insertion. The ratio of potential changes at the two ends of the fiber in the central-pool region can be obtained from the ratios $53.6/51.4 = 1.043$ and $53.0/50.7 = 1.045$ (average value, 1.044).
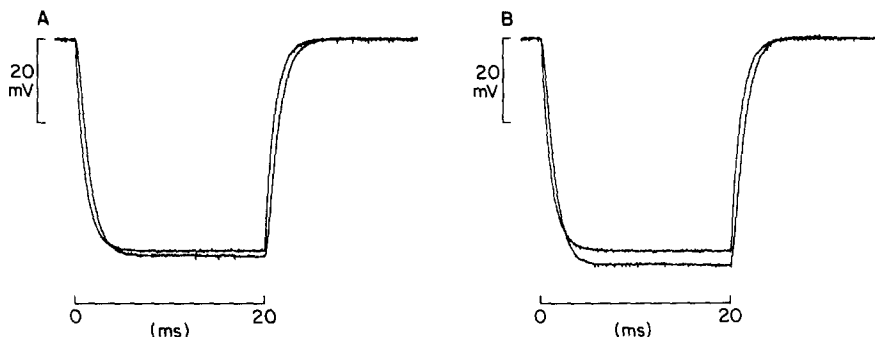

FIGURE 9. Measurements of membrane hyperpolarization under voltage clamp. Each panel shows records, taken with a 10-kHz eight-pole Bessel filter, of end-pool potential V_1 and the microelectrode potential associated with a 20-ms hyperpolarization. In A, the microelectrode was inserted into the fiber in the central-pool region 75 μm from the Vaseline seal next to EP_1; in B, it was inserted 35 μm from the seal next to EP_2. In each panel, the microelectrode record is the one with the larger final amplitude. The microelectrode was filled with 3 M KCl and had a resistance of 7 MΩ in Ringer's solution at room temperature. Since Ag paint shielding was not used, the response of the microelectrode was slower than that of the end pool. Fiber diameter, 76 μm; sarcomere spacing, 4.1 μm; Ringer's solution; temperature, 18.6–18.7°C; holding potential, -90 mV; time after saponin treatment, 30 min in A and 35 min in B; fiber 101084.1.

This experimentally measured ratio can be compared with the theoretical ratio $\Delta V_{i,b}/\Delta V_{i,a}$ for the muscle segment in the central pool (see Appendix):

$$\Delta V_{i,b}/\Delta V_{i,a} = \cosh(L_2/\Lambda_2) + \frac{r_i}{r_e + r_i} \cdot \frac{L_2}{L_1} \cdot \left[f(L_1/\Lambda_1) \cdot \frac{\sinh(L_2/\Lambda_2)}{L_2/\Lambda_2} \right], \quad (A34)$$

in which $f(L_1/\Lambda_1)$ is defined by

$$f(L_1/\Lambda_1) = \frac{L_1/\Lambda_1}{\tanh(L_1/\Lambda_1)}. \quad (A13)$$

L_1 and L_2 are the lengths of the Vaseline seals and the central-pool region, respectively. Λ_1 and Λ_2 are the corresponding space constants of the fiber, which depend on r_m and r_i and, in the case of Λ_1, r_e. For the fiber in Fig. 9, $r_m = 1.302$ M$\Omega \cdot$cm, $r_i = 4.757$ MΩ/cm, and $r_e = 205.73$ MΩ/cm. The first term on the right-hand side of Eq. A34 gives the ratio expected if the left-hand Vaseline seal provided perfect insulation and r_e were infinite; this gives $\cosh(L_2/\Lambda_2) = 1.005$. The second term, which arises because r_e is not infinite, has a value of 0.040.

Since the expression in square brackets is approximately unity, this value depends mainly on the ratios r_i/r_e and L_2/L_1 and is relatively independent of r_m. Thus, the theoretical ratio $\Delta V_{i,b}/\Delta V_{i,a}$ is equal to $1.005 + 0.040 = 1.045$, which is similar to the measured ratio 1.044, and the magnitude of the voltage increment (i.e., the amount by which $\Delta V_{i,b}/\Delta V_{i,a}$ exceeds unity) is primarily due to the second term in Eq. A34.

The experiments in Figs. 8 and 9 show that estimates of $r_e/(r_e + r_i)$ obtained from linear cable analysis agree well with values obtained from direct measurement with a microelectrode. In the central region of a cut fiber, the internal potential shows a slight variation with distance, which is greater than that expected for a terminated cable (cosh term only). This extra variation is due to the imperfect electrical insulation under the Vaseline seal; in the experiment in Fig. 9, this contributed a 4% change to ΔV from one end of the central-pool region to the other.

Optical Measurements

Wavelength dependence of resting intrinsic absorbance. Throughout this series of articles, the term absorbance, as defined by Eq. 1, is used empirically to describe the relationship between incident and transmitted light. The ratio of these two intensities depends on the optical apparatus; in particular, since light scattered by a fiber may not be collected by the measuring system, the observed ratio depends on the numerical aperture (NA) of the condensing and collecting objectives. In the experiments described here, the condensing objective NA was 0.4 and the collecting objective NA was 0.6.

Fig. 10A shows the wavelength dependence of resting intrinsic absorbance in a typical fiber. The circles represent data collected using mode 1 recording (Fig. 3) and the curve represents a least-squares fit of the empirical equation

$$A(\lambda) = a + b(550 \text{ nm}/\lambda)^m, \tag{19}$$

with $a = 0.01376$, $b = 0.01474$, and $m = 3.1$. Eq. 19 fits the wavelength dependence of resting absorbance, especially at short wavelengths, better than the simpler λ^{-m} relationship (fitted best to this set of data with $m = 1.36$) used by Baylor et al. (1982a). The improved fit by Eq. 19 is not thought to represent a difference between cut and intact fibers.

Columns 2–4 of Table III give values of a, b, and m obtained from 15 fibers in which resting absorbance was measured at five or more wavelengths early in the experiment. The average values of a, b, and m were 0.0146, 0.0154, and 4.1, respectively. On the other hand, an average value of $m = 1.23$ (0.07 SEM) was obtained on the same fibers using the simpler λ^{-m} relationship.

These results are similar to those reported for intact fibers in which the numerical apertures of the condensing and collecting objectives were comparable to those used here. Baylor et al. (1982a) found an average value of 0.028 for $A(570)$ in intact fibers. The average value in cut fibers, calculated using Eq. 19 and the mean values of a, b, and m given in Table III, is also 0.028. In a recent study, Baylor et al. (1986) measured $A(810)$ in intact fibers; the average values were 0.022 for 0° light and 0.016 for 90° light, giving 0.018 for $A(810, 1:2)$.

The value of A(810, 1:2) in cut fibers, obtained from Eq. 19 and the mean values in Table III, is exactly the same. Baylor et al. (1986) also determined the wavelength dependence of resting absorbance, using the simpler λ^{-m} relationship. Their average values of m were 1.1 for 0° light and 1.3 for 90° light (480 ≤ λ ≤ 810 nm). The average value for the fibers in Table III, based on 1:2 absorbances, was 1.23 (0.07 SEM) (420 ≤ λ ≤ 810 nm). Thus, it seems safe to conclude that freshly prepared cut and intact fibers have the same resting intrinsic absorbance.
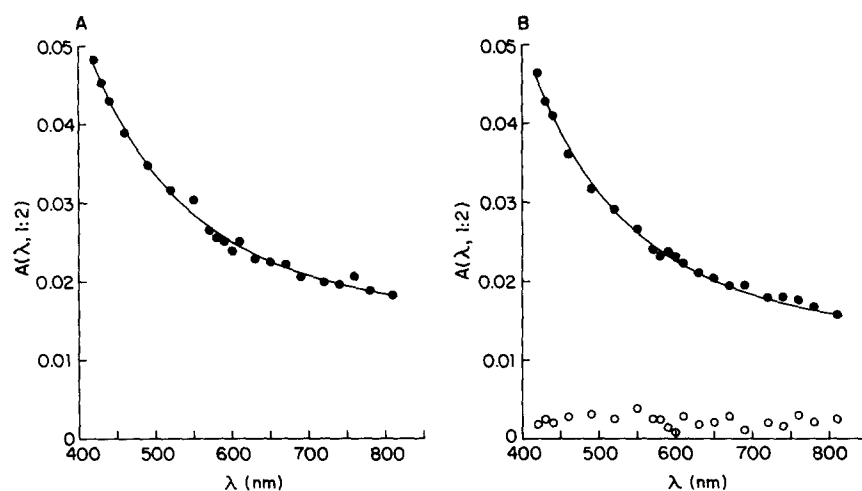

FIGURE 10. Wavelength dependence of resting intrinsic absorbance. Resting absorbance (filled circles) was measured 19–23 (A) and 78–82 min (B) after saponin treatment. The curves show least-squares fits of Eq. 19; in A, $m = 3.1$, $a = 0.01376$, $b = 0.01474$; in B, $m = 3.1$, $a = 0.01123$, $b = 0.01488$. The open circles in B give the difference between the filled circles in A and those in B. Mode 1 recording was used (Fig. 3); absorbances are plotted as 1:2 averaged values (i.e., values averaged using one part 0° polarization and two parts 90° polarization); fiber diameter, 95–96 μm in A and 96 μm in B; sarcomere spacing, 3.9 μm; Ringer's solution; temperature, 17.2–17.4°C in A and 17.9–18.0°C in B; holding potential, −90 mV; fiber 071284.1.

Changes in resting intrinsic absorbance during the course of an experiment. The filled circles in Fig. 10B show resting absorbance measured ~1 h after the data in Fig. 10A had been taken. The absorbance decreased somewhat during the interval, and the parameters obtained by fitting Eq. 19 (continuous curve) were $a = 0.01123$, $b = 0.01488$, and $m = 3.1$. The change in absorbance at each wavelength, A minus B, has been plotted as open circles in Fig. 10B; this shows no clear wavelength dependence, as expected from the relative constancy of b and m.

Accurate measurements of resting absorbance rely on a stable light source, and in experiments where this was important, such as in Fig. 10, long warm-up periods were used. The intensity of incident light was measured at the beginning

of the experiment in Fig. 10 and at the end, 135 min later; in the wavelength range 420–810 nm, it decreased, on average, by 0.09%. Intensity at intermediate times was estimated by linear interpolation. Any error introduced by this procedure should be small; a mistake of 0.09% in the intensity of incident light would change absorbance by 0.0004 units, an amount severalfold smaller than the difference shown by the open circles in Fig. 10B.

In two other experiments (not shown), resting absorbance was monitored for an extended period in the absence of indicator. After 1 h, one fiber showed a decrease in absorbance of 0.002, independent of wavelength, and the other showed an increase that varied from 0.007 at 810 nm to 0.017 at 430 nm.

TABLE III

Resting and Active Intrinsic Absorbance in Cut Muscle Fibers

(1) Fiber reference	(2) a	(3) b	(4) m	(5) $\Delta A(810)$	(6) n
061484.2	0.0186	0.0108	3.5	-1.52×10^{-4}	0.52
061584.2	0.0224	0.0120	4.5	—	—
061984.2	0.0149	0.0171	6.4	-3.87×10^{-4}	1.97
062684.1	0.0190	0.0217	3.1	—	—
070584.1	0.0105	0.0121	4.2	—	—
070584.2	0.0118	0.0130	4.3	-3.59×10^{-4}	0.99
070984.1	0.0173	0.0094	5.5	-1.11×10^{-4}	0.72
071184.1	0.0103	0.0083	5.3	-0.54×10^{-4}	0.83
071184.2	0.0133	0.0148	4.2	-1.65×10^{-4}	1.18
071284.1	0.0112	0.0200	3.1	-2.00×10^{-4}	1.06
071284.2	0.0118	0.0167	3.4	—	—
092584.1	0.0234	0.0109	5.5	-1.55×10^{-4}	1.19
092584.2	0.0123	0.0164	2.7	-5.12×10^{-4}	1.35
100384.1	0.0164	0.0160	3.9	—	—
111684.1	0.0058	0.0317	1.8	—	—
Mean	0.0146	0.0154	4.1	-2.33×10^{-4}	1.09
SEM	0.0013	0.0015	0.3	0.50×10^{-4}	0.14

Column 1 gives fiber reference; columns 2–4 give parameters in Eq. 19 that give least-squares fits to the resting absorbance data; columns 5 and 6 give parameters from Eq. 20 that give least-squares fits to the active absorbance data associated with a single action potential. Absorbance measurements on each fiber were made at five or more different wavelengths (420 ≤ λ ≤ 810 nm) 16–46 min (average value, 28 min) after saponin treatment. Fiber diameters, 70–118 µm; sarcomere spacings, 3.5–4.5 µm; Ringer's solution; average temperature, 18.0°C; holding potential, −90 mV.

Resting retardation. Mode 2 recording (Fig. 3) was used to measure resting retardation in six intact and nine cut fibers. As found by Baylor and Oetliker (1977*b*), retardation is nearly independent of wavelength in the visible range. Column 3 of Table IV gives values of resting retardation, averaged from simultaneous measurements made at three different wavelengths, and column 4 gives values of resting birefringence, equal to retardation divided by the path length (assumed to be equal to the fiber diameter). The average value of birefringence was 2.09 × 10^{-3} in six intact fibers and 1.75 × 10^{-3} in nine cut

fibers. These two values are significantly different at the level $0.01 < P < 0.025$ using the two-tailed t test.

Our value of birefringence in intact fibers is slightly smaller than that reported by Baylor and Oetliker (1977*b*), 2.25×10^{-3}, perhaps because the method used here gives the average retardation over the 50-μm illuminated spot rather than the maximum value at the thickest part of the fiber cross-section.

TABLE IV

Resting and Active Retardation in Intact and Cut Muscle Fibers

(1) Fiber reference	(2) Diam- eter	(3) Resting retard- ation	(4) Resting birefrin- gence	(5) Peak retard- ation	(6) Peak birefrin- gence	(7) Steady retard- ation	(8) Steady birefrin- gence	(9) Time to half- peak	(10) Half- width
	μm	nm	10^{-3}	nm	10^{-6}	nm	10^{-6}	ms	ms
(A) Intact fibers									
042883.1	69	133.3	1.93	−0.254	−3.68	−0.037	−0.54		14.8
042983.1	65	126.5	1.95	−0.154	−2.37	0.001	0.02		7.8
050383.1	90	170.3	1.89	−0.248	−2.76	0.030	0.33		9.2
050683.1	82	153.8	1.88	−0.184	−2.24	0.002	0.02		10.9
050683.2	108	257.8	2.39	−0.343	−3.18	−0.089	−0.82		14.2
051183.2	94	237.3	2.52	−0.363	−3.86	−0.043	−0.46		22.5
Mean	85		2.09		−3.02		−0.24		13.2
SEM			0.12		0.27		0.18		2.2
(B) Cut fibers									
061284.1	94	162.6	1.73	−0.222	−2.36	−0.021	−0.22	3.76	12.7
061484.3	86	151.9	1.77	−0.179	−2.08	−0.028	−0.33	3.51	9.2
092684.1	80	127.3	1.59	−0.129	−1.61	−0.019	−0.24	3.24	10.5
100284.1	87	158.4	1.82	−0.167	−1.92	−0.011	−0.13	3.44	7.6
101784.2	102	186.7	1.83	−0.312	−3.06	−0.056	−0.55	4.85	18.0
101884.1	71	97.3	1.37	−0.105	−1.48	−0.013	−0.18	3.17	12.5
101984.1	104	202.4	1.95	−0.224	−2.15	−0.039	−0.38	3.49	10.4
102284.2	98	174.3	1.78	−0.270	−2.76	−0.039	−0.40	3.68	10.6
102384.2	77	145.8	1.89	−0.169	−2.19	−0.021	−0.27	3.27	8.6
Mean	89		1.75		−2.18		−0.30	3.60	11.1
SEM			0.06		0.17		0.04	0.17	1.0

Column 1 gives fiber reference and column 2 gives diameter. Columns 3, 5, and 7 give resting retardation, the peak change after an action potential, and the steady level recorded 0.7–0.9 s after stimulation. Columns 4, 6, and 8 give resting, peak, and steady birefringence, obtained by dividing columns 3, 5, and 7 by column 2. Column 9 gives the time that elapsed between the time to half-peak of the action potential and the time to half-peak of the retardation signal. Column 10 gives the half-width of the retardation signal. The results in columns 3–10 are average values obtained at two or three wavelengths. The measurements on cut fibers were made 13–23 min after saponin treatment. Sarcomere spacing, 3.7–4.2 μm; Ringer's solution; average temperature, 16.7°C in A and 17.6°C in B; holding potential, −90 mV.

Optical changes after action potential stimulation measured in modes 1 and 2. Fig. 11 shows two sets of traces, one recorded in mode 1 (left-hand side) and the other recorded in mode 2 (right-hand side). In each set, the top trace shows the action potential, attenuated in amplitude as expected for the 0.625-kHz Bessel filter. The remaining traces show the outputs from the six photodiode circuits

scaled according to resting transmitted light. The optical changes occurred more slowly than the action potential and were not noticeably attenuated by the 0.625-kHz Bessel filters (see below, Fig. 16).

In mode 1, the optical traces have been scaled according to Eq. 2 so that the signals represent changes in absorbance. All six traces, representing three wavelengths and two planes of linear polarization, have similar waveforms and differ mainly in amplitude.
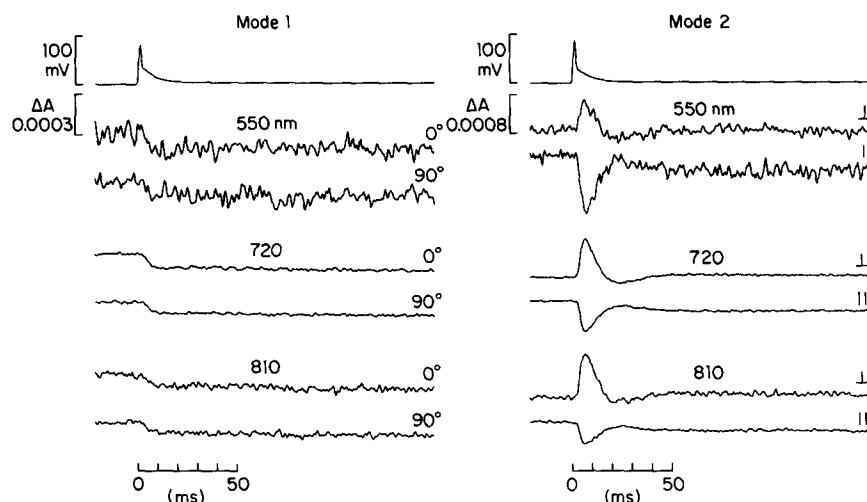

FIGURE 11. Optical changes recorded simultaneously by six photodiodes (Fig. 2) that monitor transmitted light intensity at three different wavelengths and two planes of linear polarization. Mode 1: changes in the intensity of transmitted light scaled according to Eq. 2 and plotted as changes in absorbance for 0° and 90° light at the indicated wavelengths. The top trace shows the action potential. In this and subsequent figures, its magnitude was reduced by a 0.625-kHz eight-pole Bessel filter. The actual magnitude, measured on a storage oscilloscope, was 136 mV. Mode 2: changes in intensity of transmitted light polarized perpendicular (⊥) and parallel (∥) with respect to the incident light. These signals are expressed as changes in absorbance using Eq. 2 with θ replaced with ⊥ and ∥. The resting intensities of ⊥ and ∥ transmitted light at each wavelength depend mainly on the resting retardation of the fiber (Eqs. 3 and 4) and the different transmission and reflection coefficients of the beam-splitting cubes (see Methods). For these and other reasons, normalizing the optical records by resting intensity (Eq. 2) produces different peak amplitudes and noise levels in the ⊥ and ∥ traces at each wavelength. Both mode 1 and mode 2 measurements were made on the same fiber; fiber diameter, 86 μm; sarcomere spacing, 3.8 μm; resting retardation, 152 nm; Ringer's solution; temperature, 20.4°C (mode 1) and 17.7°C (mode 2); holding potential, −90 mV; fiber 061484.3. The traces in mode 1 were taken 10 min after saponin treatment; the traces in mode 2 were taken 20 min after saponin treatment.

In mode 2, the traces have also been scaled by resting transmitted intensity times [−ln(10)], which is similar to Eq. 2. Although the vertical scale is labeled in absorbance units, the optical signals reflect changes in both absorbance and retardation. A change in true fiber absorbance (or scattering) changes the

intensity of $\perp$ and $\parallel$ light in the same direction, whereas a change in retardation produces intensity changes in opposite directions for the two polarizations (Eqs. A17 and A21 in Baylor et al., 1984). The results show that the early optical transient is due primarily to a change in retardation.

Fig. 12 shows processed optical traces from the experiment in Fig. 11. In mode 1, the average of the 0° and 90° absorbance changes is labeled "1:1." The difference between the 0° and 90° changes, called the dichroic signal, is labeled "δ." In mode 2, the original traces are combined to give the change in 1:1 absorbance (Eq. 10) and the change in optical retardation, labeled "R" (Eqs. 14 and 6). According to the theory, the absorbance signal is not contaminated by the retardation signal and vice versa. The changes in 1:1 absorbance determined
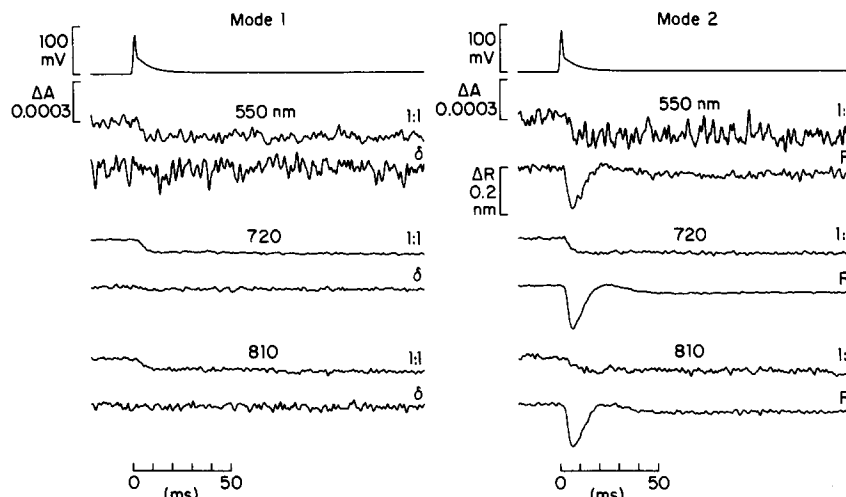
FIGURE 12. Processed optical traces from Fig. 11. Mode 1: the average of the raw 0° and 90° absorbance records is denoted by 1:1 (to indicate one part 0° polarization and one part 90° polarization) and the difference is denoted by δ. Mode 2: Eq. 10 has been used to calculate the average absorbance trace (labeled "1:1") and Eqs. 6 and 14 have been used to calculate the retardation trace (labeled "R").

in modes 1 and 2 are similar, although measurements made in mode 2 are noisier than those in mode 1 because the polarizer (POL in Figs. 2 and 3) removes 55–65% of the light.

The main conclusions from Fig. 12 are that (*a*) the changes in 1:1 absorbance follow the same waveform, but with different amplitudes, at the three wavelengths; (*b*) the dichroic traces are nearly flat; and (*c*) the retardation changes are similar at the three wavelengths. Similar results have been obtained in intact fibers (Baylor and Oetliker, 1977*b*; Baylor et al., 1982*a*). The only consistent difference we have observed is that the early transient absorbance increase usually seen after stimulation of intact fibers (Figs. 7*C*, 7*D*, 8*A*, and 9*A* in Baylor et al., 1982*a*) is rarely seen in cut fibers. The reason for this is not known.

Wavelength dependence of the active intrinsic absorbance signal. The experiment in Figs. 11 and 12 and others show that after single action potential

stimulation, the change in absorbance of a highly stretched cut fiber has the
same temporal waveform at different wavelengths. The relative amplitudes at
two wavelengths can be determined by scaling one signal to match the other.
The circles in Fig. 13A show the factors that scale the 810-nm 1:1 trace in Fig.
12, mode 1, to give least-squares fits of the 550- and 720-nm traces. The curve
labeled a was obtained from the relationship

$$\Delta A(\lambda)/\Delta A(810) = (810 \text{ nm}/\lambda)^n, \tag{20}$$

with the best-fit value $n = 0.62$. The inset in the upper right shows the 810-nm
trace superimposed with appropriately scaled versions of the 550- and 720-nm
traces.
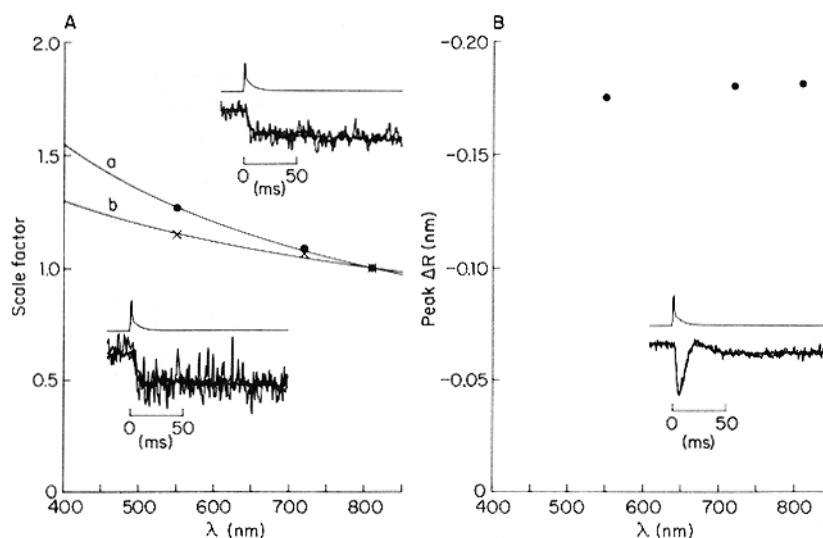
FIGURE 13.   Wavelength dependence of the changes in intrinsic absorbance and
retardation associated with one action potential. (A) Absorbance. The 810-nm 1:1
absorbance traces in Fig. 12 were scaled to give a least-squares fit to the 720- and
550-nm traces. The filled circles show the wavelength dependence of the scaling
factors obtained with mode 1. The curve labeled a was computed from Eq. 20 using
$n = 0.62$. The inset at the upper right shows the action potentials and superimposed
traces at the three wavelengths, with each trace reduced by the appropriate scaling
factor. The X's (curve b) and the inset at the lower left were obtained using mode
2, $n = 0.37$. (B) Retardation. The peak change in retardation in the traces in Fig.
12, mode 2, is plotted against wavelength. The inset shows the action potential and
retardation traces superimposed, without scaling.

The X's in Fig. 13A show the scaling factors obtained from the 1:1 traces in
Fig. 12, mode 2. The curve labeled b was drawn from Eq. 20 using the best-fit
value $n = 0.37$. The lower left-hand inset shows the three traces, scaled and
superimposed. Within the noise level, the traces are the same.

In fibers containing a Ca indicator, absorbance measurements are usually
expressed as 1:2 averages so that any effects associated with the orientation of
the indicator molecules are eliminated; this convention has also been followed

for further analysis of intrinsic signals. Because the intrinsic dichroic signals are very small (mode 1 in Fig. 12), the intrinsic 1:1 and 1:2 absorbance averages are similar. Table III gives information about active intrinsic $\Delta A(\lambda, 1{:}2)$ signals recorded, using mode 1, from nine freshly prepared cut fibers. Column 5 gives the peak magnitude of $\Delta A(810, 1{:}2)$. The average value, -2.33×10^{-4}, is within the range for intact fibers given by Baylor et al. (1982a), -0.5×10^{-4} to -3×10^{-4}. Column 6 gives the value of n in Eq. 20; its average value was 1.09, with a range of 0.52–1.97.

Changes in the active intrinsic absorbance signal during the course of an experiment. Quite frequently, the magnitude of the active intrinsic signal as well as its wavelength dependence (i.e., the parameter n in Eq. 20) changed during the course of an experiment. There is a suggestion of this in the experiment in Fig. 13A. As time progressed, the magnitude of $\Delta A(810)$ increased, as evidenced by the fact that the amplitude of the traces in the lower left-hand inset is greater than that in the upper right-hand inset, recorded 10 min earlier, and the power n decreased, as evidenced by the fact that curve b is less steep than curve a.

Another example is shown in Fig. 14A. The lower 720- and 810-nm traces have larger amplitudes than the upper traces taken 10 min earlier. During the course of the experiment, eight sets of records were taken. The circles in Fig. 14B give the scaling factors associated with the first four sets and the X's give the factors associated with the last four sets. During the run, the wavelength dependence parameter n increased; curve b was drawn from Eq. 20 with $n = 1.0$, and curve a was drawn with $n = 1.4$.

The cause of the variation in the intrinsic signal is not known. One possibility is movement artifact; fibers may become less well immobilized as an experiment progresses. In a few fibers, resting sarcomere spacing was measured at the optical recording site several times during the experiment. No changes were detected, although in some cases the amplitude of the intrinsic signal increased, as in Figs. 13 and 14. Small changes in sarcomere spacing at the optical site may not have been detected, however, and the possibility of changes elsewhere, such as under the Vaseline seals, was not investigated. Until movement can be ruled out, it would be premature to attach much significance to this variation in the intrinsic signal.

Active retardation signals. The circles in Fig. 13B show the wavelength dependence of the peak amplitude of the active retardation signal in Fig. 12, mode 2. The inset shows the three traces superimposed. Within experimental error, the change in retardation is independent of wavelength between 550 and 810 nm, as reported for intact fibers by Baylor and Oetliker (1977b) and Baylor et al. (1984).

Column 5 in Table IV gives the peak value of the retardation change that accompanied a single action potential in six intact fibers and in nine cut fibers soon after treating the end-pool regions with saponin. Column 6 gives the peak change in birefringence. The average value in intact fibers, -3.02×10^{-6}, is smaller than the value -3.78×10^{-6} reported by Baylor and Oetliker (1977b), but the difference is not statistically significant. The average value in cut fibers, -2.18×10^{-6}, is smaller than that in intact fibers, -3.02×10^{-6}, and this difference is significant at the level $0.005 < P < 0.01$ using the two-tailed t test.

Columns 7 and 8 in Table IV give the steady levels of retardation and birefringence measured 0.7–0.9 s after stimulation. In both intact and cut fibers, the average maintained change was negative; in cut fibers, the change was negative in every experiment.

The half-width of the retardation signal, given in column 10 of Table IV, is similar in intact fibers and in cut fibers studied soon after saponin treatment. In intact fibers, its average value was 13.2 ms; in cut fibers, it was 11.1 ms. These numbers are not significantly different.
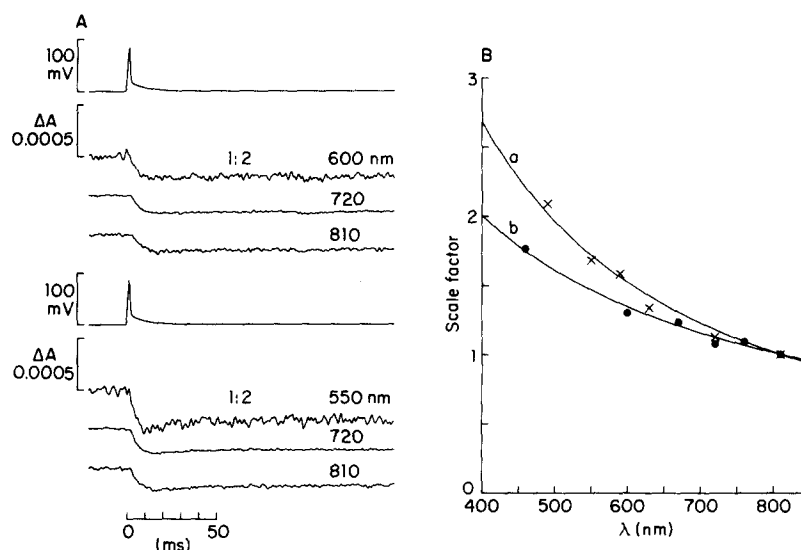
FIGURE 14.   Wavelength dependence of the changes in intrinsic absorbance. (A) Action potentials and changes in 1:2 absorbance recorded 28 min (upper set) and 38 min (lower set) after saponin treatment. (B) Scale factors obtained, as in Fig. 13, from the traces in A and others. The filled circles are from records taken 26–29 min after saponin treatment; the X's are from records obtained 30–39 min after treatment. Curves a and b were plotted from Eq. 20 using $n = 1.4$ and 1.0, respectively. Fiber diameter, 80 μm; sarcomere spacing, 4.1 μm; Ringer's solution; temperature, 19.0–19.3°C; holding potential, −90 mV; actual amplitude of the action potential, 138 mV at the beginning of the experiment and 135 mV at the end; fiber 071184.2.

Changes in the active retardation signal during the course of an experiment. Unexpectedly, the retardation signal varied considerably during the time course of many cut fiber experiments. Fig. 15A shows records from the only experiment in which measurements were made for an extended period without an indicator inside the fiber. The top pair of traces shows action potentials recorded 18 and 117 min after saponin treatment. In this interval, the peak amplitude declined slightly, from 134 mV in a to 130 mV in d, and the afterpotential became slightly more negative. Other electrical parameters were monitored and they also remained relatively constant. The holding current increased in magnitude from −83 nA in a to −93 nA in d; r_m increased from 0.071 to 0.072 MΩ·cm; $r_e/(r_e +$

r_i) decreased from 0.962 to 0.950. Thus, the electrical condition of the fiber was stable throughout the experiment.

The optical traces a–d in Fig. 15A show retardation signals recorded during the same experiment. The first trace (a) shows an early decrease in retardation that rapidly decayed to a smaller maintained level. This waveform is typical of
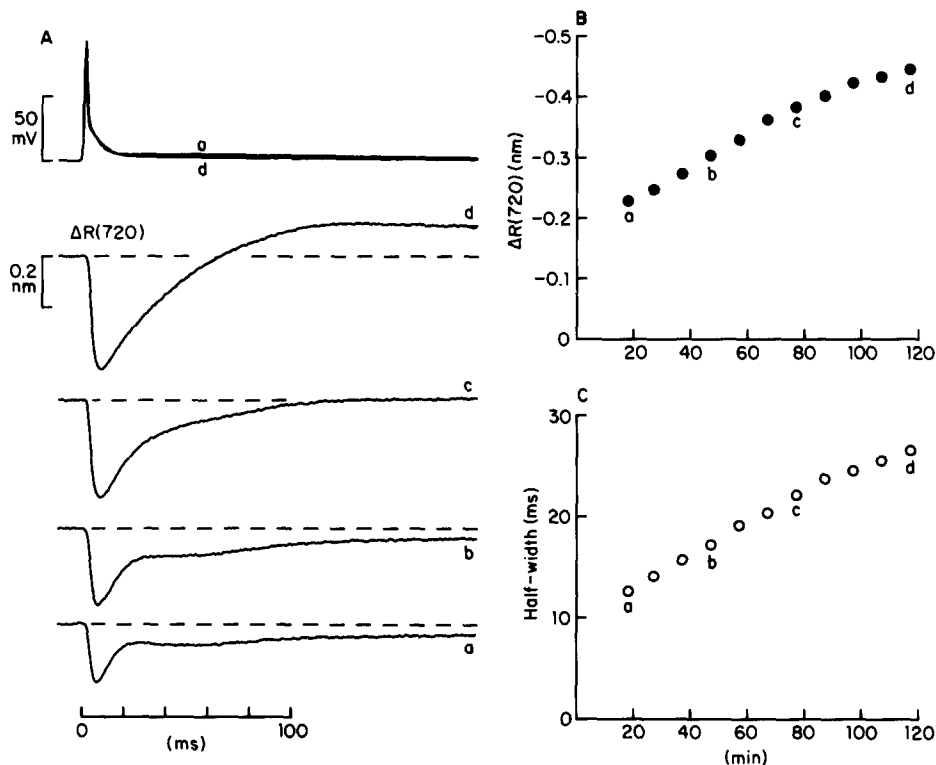

FIGURE 15. Variation in the retardation signal during the course of a single experiment. (A) Two records of the action potential, superimposed, and four traces of $\Delta R(720)$. The letters a–d are used to reference measurements made at four different times. The actual amplitude of the action potential was 134 mV at the beginning of the experiment (a) and 130 mV at the end (d). (B and C) Peak amplitude and half-width of the retardation signal plotted against time after saponin treatment. Resting retardation (average of values at 550, 720, and 810 nm) was 163 nm at a, 167 nm at b, 169 nm at c, and 172 nm at d. Fiber diameter, 94 μm at the beginning of the experiment and 86 μm at the end; sarcomere spacing, 4.1 μm; Ringer's solution; temperature, 16.3–16.5°C; holding potential, −90 mV; fiber 061284.1.

those obtained soon after saponin treatment (Table IVB). As the experiment progressed (traces b–d), the amplitude of the early peak became larger, the half-width increased, and the maintained signal reversed direction. In contrast, the time course of the rising phase remained relatively constant; the time to half-peak of ΔR after that of the action potential was 3.69 ms in a, 3.76 ms in b, 3.66

ms in c, and 3.57 ms in d. Similarly, resting retardation showed little change; it increased slightly from 163 nm in a to 172 nm in d. Fig. 15, B and C, shows plots of peak amplitude and half-width, respectively, of the retardation transient against experiment duration. These rather marked changes in ΔR are probably due to an alteration in the internal state of cut fibers during the time course of an experiment (see Discussion). As far as we are aware, such changes have not been observed in intact fibers (Baylor and Oetliker, 1977a, b).

A protocol similar to that in Fig. 15 was followed in seven other experiments in which retardation signals were monitored for 44–209 min after saponin treatment and in the presence of either arsenazo III, antipyrylazo III, tetramethylmurexide, or phenol red. The peak amplitude of $|\Delta R|$ initially increased in all seven fibers. The half-width increased in six fibers; in the seventh fiber, the early decrease in ΔR was cut short by a large, positive maintained signal, more marked than that in trace d in Fig. 15A. The changes in peak ΔR and half-width shown in Fig. 15 are therefore fairly typical of results from cut fibers.

On the other hand, a change in the steady level of ΔR, such as that shown in Fig. 15A, was found in only three fibers; the other five fibers showed little or no change. The presence of such a change was always correlated with a change in the steady level of the intrinsic absorbance signal, ΔA, which, as discussed above, may reflect a movement artifact. In contrast, the increase in peak amplitude and half-width of ΔR was observed consistently and was not necessarily correlated with any change in ΔA; for example, in one experiment (not shown), the peak ΔR changed from -0.17 to -0.25 nm and the half-width increased from 7.4 to 19.1 ms, although the intrinsic absorbance signal remained essentially constant.

Effect of filtering the optical signals. The electrical records in Fig. 8C showed that a 10-kHz, eight-pole Bessel filter delayed the action potential with almost no attenuation, whereas the 0.625-kHz Bessel filter both delayed and attenuated the signal. Since 0.625-kHz Bessel filters were routinely used in experiments with Ca indicators to improve the signal-to-noise ratio of optical signals, it was important to establish that they did so without distorting the waveforms. Tests were made using tetramethylmurexide, which gives a Ca signal more rapid in onset and briefer in duration than either arsenazo III or antipyrylazo III (Maylie et al., 1987a). Consequently, its optical signals should be most vulnerable to distortion by the 0.625-kHz filter.

Fig. 16A shows electrical and optical traces from a fiber that contained tetramethylmurexide. Three sets of records were obtained in sequence, using 0.625-, 10-, and 0.625-kHz filters. The top set of traces shows the action potential; the next set shows $\Delta A(570, 1{:}2)$, an absorbance change that is sensitive to Ca; and the lower set shows the intrinsic signal $\Delta A(690, 1{:}2)$. Since 10- and 0.625-kHz eight-pole Bessel filters are expected to shift the temporal waveform by 0.1 and 1.6 ms, respectively, the traces in Fig. 16A should be compared by shifting the 10-kHz traces 1.5 ms to the right.

Fig. 16B shows the shifted 10-kHz traces superimposed on the averaged 0.625-kHz traces. The two action potential records are markedly different, as expected from Fig. 8C. The 10-kHz record has a peak amplitude of 134 mV, whereas the 0.625-kHz record has a peak amplitude of 108 mV. Although the temporal

waveform of the action potential was distorted by the 0.625-kHz filter, the time to half-peak on the rising phase still provides a reliable measure of timing; this point was reached 1.3 ms later with the 0.625-kHz filter than with the 10-kHz filter, a delay close to the expected 1.5 ms. The 570- and 690-nm absorbance
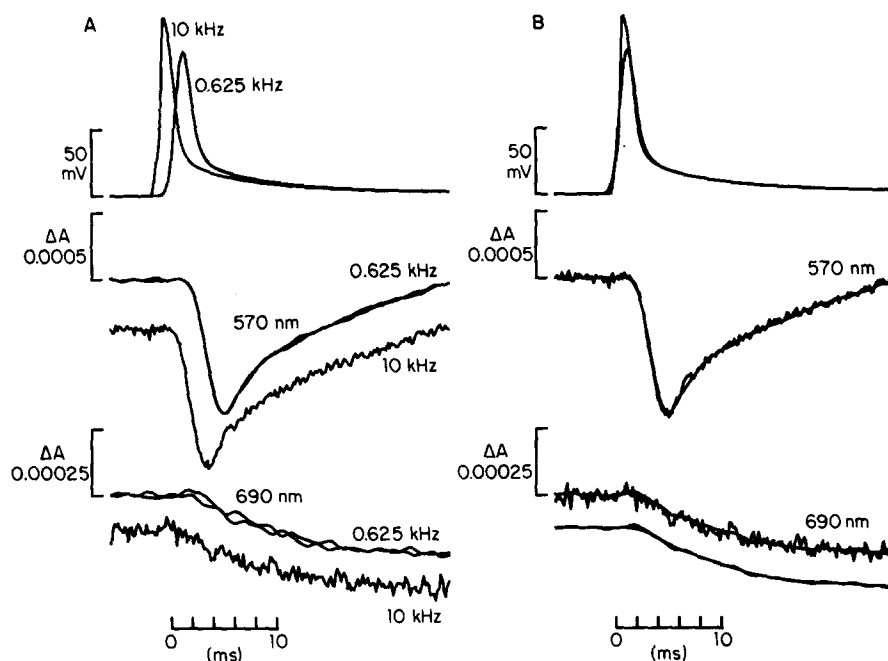

FIGURE 16. The effect of filtering the action potential and the optical signals from a fiber containing the Ca indicator tetramethylmurexide. (A) Traces obtained with 0.625-, 10-, and 0.625-kHz eight-pole Bessel filters; sampling rate, 100 kHz; the bracketing 0.625-kHz measurements are superimposed. The upper three records (all superimposed) show the action potential, the middle traces show $\Delta A(570, 1:2)$, and the lower traces show $\Delta A(690, 1:2)$. (B) Comparison of the averaged traces in A recorded with 0.625-kHz filters and the traces recorded with the 10-kHz filters but shifted 1.5 ms to the right to compensate for the different low-frequency time delays of the two filters. The first pair of traces shows the action potential, the second pair shows $\Delta A(570, 1:2)$, and the third pair shows $\Delta A(690, 1:2)$. The fourth pair shows the 0.625-kHz $\Delta A(690, 1:2)$ averaged signal again, and the same signal filtered by a 0.1-kHz digital Gaussian filter. Fiber diameter, 93 μm; sarcomere spacing, 3.7 μm; internal concentration of tetramethylmurexide, 3.7 mM; Ringer's solution; temperature, 18.0°C; holding potential, −90 mV; time after saponin treatment, 81–83 min; fiber 101984.1.

traces, on the other hand, were little affected by the 0.625-kHz filters, apart from the expected time shift. The peak amplitude of the $\Delta A(570, 1:2)$ signal was −0.00103 with the 10-kHz filters and −0.00101 with the 0.625-kHz filters.

In experiments with Ca indicators, described in the following three articles (Maylie et al., 1987*a–c*), the indicator-related Ca signal was obtained by subtract-

ing a scaled intrinsic signal, taken at a wavelength where the indicator does not absorb, from a signal taken simultaneously at a Ca-sensitive wavelength. Since any noise on the intrinsic signal is transferred to the corrected Ca signal, the intrinsic signal was sometimes additionally filtered by a 0.05–0.2-kHz digital Gaussian filter (Colquhoun and Sigworth, 1983). The bottom pair of traces in Fig. 16B shows the effect of this filtering. The two 0.625-kHz $\Delta A(690, 1:2)$ signals, one before and the other after 0.1-kHz Gaussian filtering, are very similar, which indicates that the Gaussian filter did not distort the time course of the change in intrinsic absorbance.

DISCUSSION

One aim of this article is to describe a new apparatus for making simultaneous optical measurements on single muscle fibers at three different wavelengths and two planes of linear polarization. Several advantages of this method will be illustrated in the following articles (Maylie et al., 1987a–c). First, in fibers that contain a Ca indicator, it is possible to determine the waveform of one or two indicator-related signals from a single set of simultaneous records made during either action potential stimulation or a voltage-clamp step. Any change in the intrinsic absorbance signal from run to run, such as frequently occurs, is automatically taken into account. Second, the number of times that a fiber needs to be stimulated is substantially reduced. With the previous method (Baylor et al., 1982a–c), six to eight stimuli were required to get a well-bracketed result, whereas the new method requires only a single stimulus. This is especially important for voltage-clamp experiments in which strong depolarizing steps are employed. Third, with mode 2, changes in absorbance and retardation can be simultaneously recorded in a straightforward manner.

Most of the experiments made with this apparatus were carried out on cut frog muscle fibers (Hille and Campbell, 1976) mounted in a double-Vaseline-gap chamber (Kovacs et al., 1983). Measurements of intrinsic absorbance, both resting and after action potential stimulation, gave results in freshly prepared cut fibers similar to those obtained previously in intact fibers. No attempt was made, however, to resolve such measurements of absorbance, defined operationally as $\log_{10}$ of the ratio of incident to transmitted light intensity, into contributions from true fiber absorbance and those from light scattering by the fiber. The wavelength dependence of resting absorbance (Fig. 10 and Table III) would be consistent with an absorbance contribution either from the presence of molecules that absorb light at short wavelengths or, since the value of m (Eq. 19) is close to 4, from Rayleigh scattering.

Several properties of the active intrinsic signal seem well established. After action potential stimulation in intact fibers, there is a small, early, and brief increase in absorbance (Baylor et al., 1982a); the experiments in this article show that this is less pronounced in cut fibers. This small increase is rapidly followed by a larger decrease in absorbance that is similar in intact (Baylor et al., 1982a) and cut (this article) fibers, and, at least in cut fibers, is maintained for at least 8 s (Fig. 6 in Maylie et al., 1987a). This absorbance decrease has a time course that is relatively independent of wavelength in the range $400 \leq \lambda \leq 800$ nm and

an amplitude that varies approximately as $1/\lambda$. The rising phase of this signal lags that of either the retardation signal (Baylor and Oetliker, 1977b; Fig. 17 in Maylie et al., 1987c) or the Ca signal (Fig. 17 in Maylie et al., 1987c). The amplitude of this signal summates with repetitive stimulation (Fig. 6 in Maylie et al., 1987a, and our unpublished observations on intact and cut fibers). A similar decrease in absorbance, with many of the above properties, has been observed in cut fibers during voltage-clamp depolarizations (Kovacs and Schneider, 1977; Kovacs et al., 1983; Melzer et al., 1986). The possible origins of this signal are discussed by Kovacs and Schneider (1977) and by Rios et al. (1983).

Our experiments showed only two differences of consequence between the optical properties of freshly prepared cut fibers and intact fibers: the resting birefringence in cut fibers is only 0.82 times that in intact fibers and the peak change after an action potential is only 0.69 times that in intact fibers. These differences may result from a small change in the anatomical properties of cut fibers, such as an increase in fiber volume during preparation, or, in the case of the active signal, changes in physiological properties.

Another possible difference between intact and cut fibers is that the waveform of the retardation signal in cut fibers can vary considerably during the course of an experiment; in one experiment, its amplitude and half-width each increased twofold in 2 h. A similar change occurs in the half-width of the Ca signal but not in its amplitude (Fig. 15 in Maylie et al., 1987c). These changes in the retardation signal, which have not been reported in intact fibers, are probably due to a progressive change in some internal properties of a cut fiber during the time course of an experiment (also see Maylie et al., 1987b, c).

This article also describes a simple way, based on linear cable theory, to estimate r_m and r_i in a cut fiber, as well as r_e under the Vaseline seals. The method, which does not require microelectrodes, can routinely monitor the electrical condition of a fiber during the course of an experiment. The values of r_m and r_i obtained from cut fibers with this method agree reasonably well with the values obtained from intact fibers using microelectrode techniques. The agreement is better with TEA solution than with Ringer's, possibly because TEA reduces nonlinearities in the membrane I-V curve that might interfere with estimates derived from linear cable theory.

APPENDIX

This section derives the relationships between the parameters a_1, a_2, and b_2, which can be measured in a saponin-treated cut fiber mounted in a double-Vaseline-gap chamber (Eqs. 15–17), and the electrical properties r_m, r_i, and r_e. r_m is the membrane resistance of the fiber for unit length, r_i is the internal resistance per unit length, and r_e is the external resistance under the Vaseline seal per unit length. The values of r_m, r_i, and r_e are assumed to be independent of distance; in particular, r_m and r_i are assumed to be the same under the seals as in the central pool.

The theoretical procedure divides the fiber into three electrical segments as diagrammed in Fig. 17. $V_{i,a}$ and $i_{i,a}$ (Fig. 17A) are each expressed as a linear combination of V_1 and I_1 plus a constant. $V_{i,b}$ and $i_{i,b}$ (Fig. 17B) are expressed as linear combinations of $V_{i,a}$ and $i_{i,a}$ plus constants, and V_2 and I_2 (Fig. 17C) are expressed as linear combinations of $V_{i,b}$ and $i_{i,b}$ plus constants. The results are then combined, using matrix algebra, to give V_2 and I_2 as linear combinations of V_1 and I_1 plus constants. If the left-hand end pool is

used to measure voltage, then $I_1 = 0$, and V_2 and I_2 are each proportional to V_1 plus a constant (Eqs. 15–16).

Seal Region of Length L_1 That Separates the Left-Hand End Pool from the Central Pool (Fig. 17A)

Current, I_1, is injected into the end pool and voltage, V_1, is measured. The internal voltage, $V_{i,a}$, and internal current, $i_{i,a}$, at the right-hand boundary of the seal can be derived as follows.
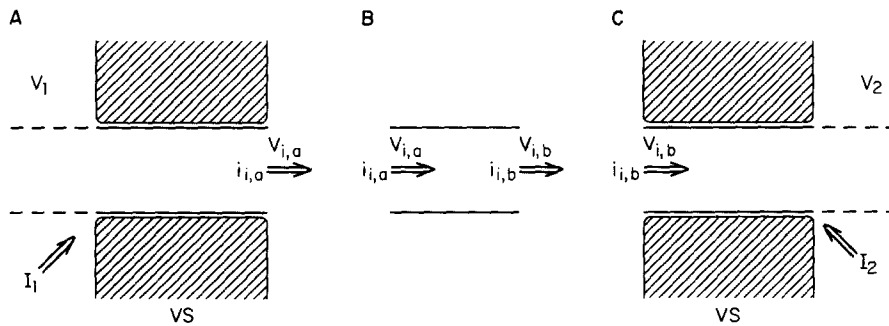

FIGURE 17. Schematic diagram showing the terminology for voltage and current used in the cable analysis of cut fibers in the double-Vaseline-gap chamber. (A) End pool EP_1 (Fig. 1) and the adjacent Vaseline seal (VS) of length L_1. V_1 represents the potential in the end pool and I_1 represents the current injected into it. The potential inside the fiber at the right-hand edge of the seal is denoted as $V_{i,a}$ and the internal longitudinal current (flowing in the direction shown) is $i_{i,a}$. (B) Central-pool region, length L_2. The left-hand edge of the fiber has internal voltage and current $V_{i,a}$ and $i_{i,a}$ (same as the right-hand edge in A); the right-hand edge has values denoted by $V_{i,b}$ and $i_{i,b}$. (C) End pool EP_2 and the adjacent Vaseline seal, length L_1. $V_{i,b}$ and $i_{i,b}$ are the same as in B. V_2 and I_2 represent the voltage and injected current in end pool EP_2. In the analysis, the external potential in the central pool is taken as zero.

The external voltage under the seal, V_e, and the internal voltage, V_i, are related to the external and internal currents, i_e and i_i, by the well-known relations

$$dV_e/dx = -r_e i_e,\qquad\qquad(A1)$$

$$dV_i/dx = -r_i i_i,\qquad\qquad(A2)$$

with the added condition that

$$I_1 = i_e + i_i.\qquad\qquad(A3)$$

The variable x represents distance along the fiber axis. Integration of Eqs. A1 and A2 from the left-hand boundary of the seal to the right-hand boundary, in com⁻ ination with Eq. A3, gives

$$V_{i,a} = \frac{r_e + r_i}{r_e}\cdot V_1 - r_i L_1 I_1.\qquad\qquad(A4)$$

This relationship, which also holds during transients, depends only on r_e and r_i and not on specific membrane properties. If the left-hand end pool is used to measure voltage, then I_1 is zero and V_1 is $r_e/(r_e + r_i)$ times the true membrane potential, $V_{i,a}$.

Eqs. A1–A3 can be combined to give

$$i_i = \frac{1}{r_e + r_i} \cdot (r_e I_1 - dV/dx), \tag{A5}$$

in which V denotes the transmembrane potential, $V_i - V_e$. The steady state solution for V can be obtained from the cable equation

$$d^2V/dx^2 = (r_i + r_e)i_m, \tag{A6}$$

in which i_m represents membrane current per unit length of fiber. This equation can be obtained by differentiating Eqs. A1–A3 and using the relationships

$$i_m = -di_i/dx, \tag{A7}$$

$$= di_e/dx. \tag{A8}$$

Eq. A6 is easily solved if the membrane is ohmic, in which case

$$i_m = (V - V_r)/r_m. \tag{A9}$$

V_r is the reversal potential, i.e., the potential that would be measured if $i_m = 0$.

Since the solutions in the end pool and central pool have very different concentrations of K and Cl, V_r will vary with x. Two types of variation have been considered.

Case 1: Linear Variation of V_r. The first case is that V_r varies linearly with distance across the Vaseline seal, being zero at the left-hand edge, where the saponin-treated region is exposed to high-K solution, and V_{RP} at the right-hand edge, where the fiber is exposed to Ringer's or TEA solution. V_{RP} is the resting potential expected in Ringer's solution, which will be taken as −90 mV. Thus,

$$V_r = (x/L_1)V_{RP}. \tag{A10}$$

The solution of Eqs. A6, A9, and A10 that satisfies the boundary conditions at $x = 0$ and $x = L_1$, $V(0) = 0$ and $V(L_1) = V_{i,a}$ (since the external potential is zero in the central pool), is

$$V = (x/L_1)V_{RP} + (V_{i,a} - V_{RP}) \cdot \frac{\sinh(x/\Lambda_1)}{\sinh(L_1/\Lambda_1)}, \tag{A11}$$

where Λ_1 is the space constant under the seal ($= [r_m/(r_i + r_e)]^{1/2}$). Eq. A11 can be differentiated and combined with Eq. A5 to give

$$i_{i,a} = \frac{r_e}{r_e + r_i} \cdot I_1 - \frac{1}{(r_e + r_i)L_1} \cdot [V_{RP} + (V_{i,a} - V_{RP}) \cdot f(L_1/\Lambda_1)], \tag{A12}$$

where

$$f(L_1/\Lambda_1) = \frac{L_1/\Lambda_1}{\tanh(L_1/\Lambda_1)}. \tag{A13}$$

Substitution of $V_{i,a}$, from Eq. A4, into Eq. A12 gives

$$i_{i,a} = -\frac{f(L_1/\Lambda_1)}{r_e L_1} \cdot V_1 + \frac{r_e + r_i f(L_1/\Lambda_1)}{r_e + r_i} \cdot I_1 - \frac{1 - f(L_1/\Lambda_1)}{(r_e + r_i)L_1} \cdot V_{RP}. \tag{A14}$$

Eqs. A4 and A14 allow $V_{i,a}$ and $i_{i,a}$ to be determined from V_1 and I_1. Using matrix notation, if the column vectors $\mathbf{Y}_1$ and $\mathbf{Y}_a$ are defined as

$$\mathbf{Y}_1 = \begin{vmatrix} V_1 \\ I_1 \end{vmatrix} \tag{A15}$$

and

$$\mathbf{Y}_a = \begin{vmatrix} V_{i,a} \\ \\ i_{i,a} \end{vmatrix}, \tag{A16}$$

then

$$\mathbf{Y}_a = \mathbf{S}\mathbf{Y}_1 + V_{RP}\mathbf{A}. \tag{A17}$$

The matrix $\mathbf{S}$ and column vector $\mathbf{A}$ are given by

$$\mathbf{S} = \begin{vmatrix} (r_e + r_i)/r_e & -r_iL_1 \\ \\ -\dfrac{f(L_1/\Lambda_1)}{r_eL_1} & \dfrac{r_e + r_if(L_1/\Lambda_1)}{r_e + r_i} \end{vmatrix} \tag{A18}$$

and

$$\mathbf{A} = \begin{vmatrix} 0 \\ \\ \dfrac{f(L_1/\Lambda_1) - 1}{(r_e + r_i)L_1} \end{vmatrix}. \tag{A19}$$

Case 2: Constant V_r. The second case considers V_r to be constant. $\mathbf{Y}_a$ is then given by

$$\mathbf{Y}_a = \mathbf{S}\mathbf{Y}_1 + V_r\mathbf{A}', \tag{A20}$$

in which the matrix $\mathbf{S}$ is unchanged and $\mathbf{A}'$ is given by

$$\mathbf{A}' = \begin{vmatrix} 0 \\ \\ \dfrac{(L_1/\Lambda_1)\sinh(L_1/\Lambda_1) + [1 - \cosh(L_1/\Lambda_1)]f(L_1/\Lambda_1)}{(r_e + r_i)L_1} \end{vmatrix}. \tag{A21}$$

Central-Pool Region of Length L_2 (Fig. 17B)

Current, $i_{i,a}$, is injected into the fiber, in the central-pool region, at the boundary with the left-hand seal where the internal potential is $V_{i,a}$. The external potential is zero. Since external [K] is constant and equal to the concentration in Ringer's or TEA solution, $V_r = V_{RP}$. Eqs. A6, with $r_e = 0$, and A9 give the internal voltage and current. The solution for V contains hyperbolic sine and cosine terms whose coefficients can be evaluated from $V_{i,a}$ and $i_{i,a}$. In matrix notation, if $\mathbf{Y}_b$ is defined as

$$\mathbf{Y}_b = \begin{vmatrix} V_{i,b} \\ \\ i_{i,b} \end{vmatrix}, \tag{A22}$$

then

$$\mathbf{Y}_b = \mathbf{F}\mathbf{Y}_a + V_{RP}\mathbf{B}. \tag{A23}$$

The matrix $\mathbf{F}$ and column vector $\mathbf{B}$ are given by

$$\mathbf{F} = \begin{vmatrix} \cosh(L_2/\Lambda_2) & -r_i\Lambda_2\sinh(L_2/\Lambda_2) \\ \\ -\sinh(L_2/\Lambda_2)/(r_i\Lambda_2) & \cosh(L_2/\Lambda_2) \end{vmatrix} \tag{A24}$$

and

$$B = \begin{vmatrix} 1 - \cosh(L_2/\Lambda_2) \\ \\ \sinh(L_2/\Lambda_2)/(r_i\Lambda_2) \end{vmatrix}, \tag{A25}$$

where the space constant $\Lambda_2 = (r_m/r_i)^{\frac{1}{2}}$.

Seal Region of Length L_1 That Separates the Central Pool from the Right-Hand Pool (Fig. 17C)

This is similar to Fig. 17A, except that the direction of current $i_{i,b}$ is reversed. If the column vector $\mathbf{Y}_2$ is defined as

$$\mathbf{Y}_2 = \begin{vmatrix} V_2 \\ \\ I_2 \end{vmatrix}, \tag{A26}$$

then comparison with Eq. A17 gives

$$\begin{vmatrix} 1 & 0 \\ 0 & -1 \end{vmatrix} \mathbf{Y}_b = S\mathbf{Y}_2 + V_{RP}\mathbf{A}, \tag{A27}$$

which can be rearranged to give

$$\mathbf{Y}_2 = S^{-1} \begin{vmatrix} 1 & 0 \\ 0 & -1 \end{vmatrix} \mathbf{Y}_b - V_{RP}S^{-1}\mathbf{A}. \tag{A28}$$

Eq. A28 applies to case 1, with linear variation of V_r under the Vaseline seal. For case 2, with constant V_r,

$$\mathbf{Y}_2 = S^{-1} \begin{vmatrix} 1 & 0 \\ 0 & -1 \end{vmatrix} \mathbf{Y}_b - V_r S^{-1}\mathbf{A}'. \tag{A29}$$

Combined Solution

Eqs. A17, A23, and A28 can be combined to give

$$\mathbf{Y}_2 = S^{-1} \begin{vmatrix} 1 & 0 \\ 0 & -1 \end{vmatrix} \left[FS\mathbf{Y}_1 + V_{RP}S^{-1} \left[\begin{vmatrix} 1 & 0 \\ 0 & -1 \end{vmatrix} (\mathbf{FA} + \mathbf{B}) - \mathbf{A} \right] \right], \tag{A30}$$

which applies to case 1, Eq. A10, in which V_r is assumed to vary linearly with distance under the Vaseline seal.

If V_r is assumed to be constant (case 2), the equation for $\mathbf{Y}_2$ is obtained from Eqs. A20, A23, and A29:

$$\mathbf{Y}_2 = S^{-1} \begin{vmatrix} 1 & 0 \\ 0 & -1 \end{vmatrix} \left[FS\mathbf{Y}_1 + V_{RP}S^{-1} \begin{vmatrix} 1 & 0 \\ 0 & -1 \end{vmatrix} \mathbf{B} + V_r S^{-1} \left[\begin{vmatrix} 1 & 0 \\ 0 & -1 \end{vmatrix} \mathbf{FA}' - \mathbf{A}' \right] \right]. \tag{A31}$$

In either case 1 or case 2, since the left-hand end pool is used for measuring potential, and hence $I_1 = 0$, these relationships between V_2, I_2, and V_1 have the same form as Eqs. 15 and 16, namely,

$$V_2 = a_1 V_1 + b_1, \tag{15}$$

$$I_2 = a_2 V_1 + b_2. \tag{16}$$

The coefficients a_1 and a_2 do not depend on the assumptions concerning the spatial variation of V_r in the gap region, whereas b_1 and b_2 do.

Variation of Potential within the Central-Pool Region

In response to a change in current, ΔI_2, the magnitude of voltage change $\Delta V_{i,a}$ will be smaller than $\Delta V_{i,b}$. The steady state ratio $\Delta V_{i,b}/\Delta V_{i,a}$ can be evaluated from the above equations. According to Eq. A23, changes in the vectors $\mathbf{Y}_a$ and $\mathbf{Y}_b$ are related by

$$\Delta \mathbf{Y}_b = \mathbf{F} \Delta \mathbf{Y}_a. \tag{A32}$$

Similarly, changes in $\mathbf{Y}_1$ and $\mathbf{Y}_a$ are related by

$$\Delta \mathbf{Y}_a = \mathbf{S} \Delta \mathbf{Y}_1 \tag{A33}$$

(Eq. A17 or A20). Since $I_1 = 0$, the two equations can be combined to obtain

$$\Delta V_{i,b}/\Delta V_{i,a} = \cosh(L_2/\Lambda_2) + \frac{r_i}{r_e + r_i} \cdot \frac{L_2}{L_1} \left[f(L_1/\Lambda_1) \frac{\sinh(L_2/\Lambda_2)}{L_2/\Lambda_2} \right]. \tag{A34}$$

The first term on the right-hand side, the cosh function, gives the ratio expected if the left-hand Vaseline seal provided perfect insulation so that r_e was infinite and $i_{i,a} = 0$. The second term gives the additional increment that occurs because $i_{i,a}$ is not zero. In most of our experiments, $f(L_1/\Lambda_1) \approx 1$ and $\sinh(L_2/\Lambda_2) \approx L_2/\Lambda_2$, so that the term inside the brackets is approximately unity.

REFERENCES

Adrian, R. D. 1983. Electrical properties of striated muscle. *In* Handbook of Physiology. Section on Skeletal Muscle. L. D. Peachey and R. D. Adrian, editors. American Physiological Society, Bethesda, MD. 275–300.

Baylor, S. M., W. K. Chandler, and M. W. Marshall. 1982a. Optical measurements of intracellular pH and magnesium in frog skeletal muscle fibres. *Journal of Physiology.* 331:105–137.

Baylor, S. M., W. K. Chandler, and M. W. Marshall. 1982b. Use of metallochromic dyes to measure changes in myoplasmic calcium during activity in frog skeletal muscle fibres. *Journal of Physiology.* 331:139–177.

Baylor, S. M., W. K. Chandler, and M. W. Marshall. 1982c. Dichroic components of arsenazo III and dichlorophosphonazo III signals in skeletal muscle fibres. *Journal of Physiology.* 331:179–210.

Baylor, S. M., W. K. Chandler, and M. W. Marshall. 1984. Calcium release and sarcoplasmic reticulum membrane potential in frog skeletal muscle fibres. *Journal of Physiology.* 348:209–238.

Baylor, S. M., S. Hollingworth, C. S. Hui, and M. E. Quinta-Ferreira. 1986. Properties of the metallochromic dyes arsenazo III, antipyrylazo III and Azo1 in frog skeletal muscle fibres at rest. *Journal of Physiology.* 377:89–141.

Baylor, S. M., and H. Oetliker. 1977a. A large birefringence signal preceding contraction in single twitch fibres of the frog. *Journal of Physiology.* 264:141–162.

Baylor, S. M., and H. Oetliker. 1977b. The optical properties of birefringence signals from single muscle fibres. *Journal of Physiology.* 264:163–198.

Baylor, S. M., M. E. Quinta-Ferreira, and C. S. Hui. 1983. Comparison of isotropic calcium signals from intact frog muscle fibers injected with arsenazo III or antipyrylazo III. *Biophysical Journal.* 44:107–112.

Colquhoun, D., and F. J. Sigworth. 1983. Fitting and statistical analysis of single-channel records. *In* Single-Channel Recording. B. Sakmann and E. Neher, editors. Plenum Press, New York. 191–263.

Eberstein, A., and A. Rosenfalck. 1963. Birefringence of isolated muscle fibres in twitch and tetanus. *Acta Physiologica Scandinavica.* 57:144–166.

Endo, M., and M. Iino. 1980. Specific perforation of muscle cell membranes with preserved SR functions by saponin. *Journal of Muscle Research and Cell Motility.* 1:89–100.

Hamming, R. W. 1977. Digital Filters. Prentice-Hall, Inc., Englewood Cliffs, NJ. 34.

Hille, B., and D. T. Campbell. 1976. An improved Vaseline gap voltage clamp for skeletal muscle fibers. *Journal of General Physiology.* 67:265–293.

Hodgkin, A. L., and S. Nakajima. 1972. The effect of diameter on the electrical constants of frog skeletal muscle fibres. *Journal of Physiology.* 221:105–120.

Jobsis, F. F., and M. J. O'Connor. 1966. Calcium release and reabsorption in the sartorius muscle of the toad. *Biochemical and Biophysical Research Communications.* 25:246–252.

Kovacs, L., E. Rios, and M. F. Schneider. 1979. Calcium transients and intramembrane charge movement in skeletal muscle fibres. *Nature.* 279:391–396.

Kovacs, L., E. Rios, and M. F. Schneider. 1983. Measurement and modification of free calcium transients in frog skeletal muscle fibres by a metallochromic indicator dye. *Journal of Physiology.* 343:161–196.

Kovacs, L., and M. F. Schneider. 1977. Increased optical transparency associated with excitation-contraction coupling in voltage-clamped cut skeletal muscle fibres. *Nature.* 265:556–560.

Maylie, J., M. Irving, N. L. Sizto, G. Boyarsky, and W. K. Chandler. 1987a. Calcium signals recorded from cut frog twitch fibers containing tetramethylmurexide. *Journal of General Physiology.* 89:145–176.

Maylie, J., M. Irving, N. L. Sizto, and W. K. Chandler. 1987b. Comparison of arsenazo III optical signals in intact and cut frog twitch fibers. *Journal of General Physiology.* 89:41–81.

Maylie, J., M. Irving, N. L. Sizto, and W. K. Chandler. 1987c. Calcium signals recorded from cut frog twitch fibers containing antipyrylazo III. *Journal of General Physiology.* 89:83–143.

Melzer, W., E. Rios, and M. F. Schneider. 1986. The removal of myoplasmic free calcium following calcium release in frog skeletal muscle. *Journal of Physiology.* 372:261–292.

Miledi, R., I. Parker, and P. H. Zhu. 1982. Calcium transients evoked by action potentials in frog twitch muscle fibres. *Journal of Physiology.* 333:655–679.

Persson, A. 1963. The negative after-potential of frog skeletal muscle fibres. *Acta Physiologica Scandinavica.* 58:Suppl. 205.

Quinta-Ferreira, M. E., S. M. Baylor, and C. S. Hui. 1984. Antipyrylazo III (Ap III) and arsenazo III (Az III) calcium transients from frog skeletal muscle fibers simultaneously injected with both dyes. *Biophysical Journal.* 45:47a. (Abstr.)

Rios, E., W. Melzer, and M. F. Schneider. 1983. An intrinsic optical signal is related to the calcium transient of frog skeletal muscle. *Biophysical Journal.* 41:396a. (Abstr.)

Stanfield, P. R. 1970. The effect of tetraethylammonium ion on the delayed currents of frog skeletal muscle. *Journal of Physiology.* 209:209–229.